Mathematical Biosciences and Engineering

https://www.aimspress.com/journal/mbe

MBE, 22(11): 2944–2987.
DOI: 10.3934/mbe.2025109
Received: 19 May 2025
Revised: 31 July 2025
Accepted: 20 August 2025
Published: 24 September 2025

Research article

Reaction-diffusion modeling of vascular tumor growth: Bifurcation, relapse, and therapy efficacy

Priscilla Owusu Sekyere[1], Majid Bani-Yaghoub[1,*] and Bi-Botti C. Youan[2]

[1] Division of Computing, Analytics & Mathematics, School of Science and Engineering, University of Missouri-Kansas City, 5100 Rockhill Rd., Kansas City, Missouri 64110, USA

[2] Laboratory of Future Nanomedicines and Theoretical Chronopharmaceutics, Division of Pharmaceutical Sciences, School of Pharmacy, University of Missouri-Kansas City, 2464 Charlotte Street, Kansas City, Missouri 64108, USA

* **Correspondence:** Email: baniyaghoubm@umkc.edu.

Abstract: The vascular tumor growth model proposed by Pinho et al. has gained attention in studies of the effect of anti–angiogenic therapy. In the present work, we extend Pinho's model to a reaction-diffusion model with different cell growth behaviors to evaluate the individual and combined effects of chemotherapy, anti–angiogenic therapy, and immunotherapy across different stages of vascular cancer. Analysis of the model includes the existence and stability of up to six different equilibria with bifurcations that define the transitions between them. By establishing conditions for the stability of the cancer-free equilibrium, we numerically explore different dynamics of cancer relapse. This includes examining the timing and frequency of relapse and identifying thresholds for critical treatment parameters. Furthermore, the numerical simulations of the extended model show that in the advanced stages of cancer, the integration of chemotherapy, immunotherapy, and anti–angiogenic therapy is essential for effective control of vascular cancer and reduces the overall duration of treatment.

Keywords: reaction–diffusion model; tumor; relapse; bifurcation; vascular cancer

1. Introduction

Growth and treatment of tumors present significant challenges in medical research, as cancerous cells not only proliferate rapidly but also interact dynamically with the surrounding tissues and the body's response mechanisms [1]. Over the past two decades, mathematical models have become essential tools in optimizing cancer treatment, simulating complex tumor dynamics, assessing treatment efficacy, and possibly refining therapeutic protocols [2]. These models are often based on ordinary, stochastic, partial, or delay differential equations (ODE, SDE, PDE, or DDE) for exploring complex

interactions among cancer cells, treatments, and immune responses [2, 3].

Vascular cancer, or angiosarcoma, is a rare and aggressive tumor that originates in the blood or lymphatic vessels [4]. It can develop in various organs, including the skin, liver, and spleen [5]. Due to its rapid spread and resistance to treatment, vascular cancer is challenging to manage, requiring early detection and a multi-modal approach, including surgery and chemotherapy [6]. Numerous modeling efforts have been devoted to understanding the dynamics of vascular cancer and evaluating the effectiveness of various treatment strategies. Table 1 provides a summary of recent models of tumor growth and their key findings. For instance, the study by Sadeghi et al. [7] demonstrated that an adaptive fuzzy sliding mode controller, optimized with a genetic algorithm, can reduce chemotherapy dosage by nearly 96% while achieving complete cancer cell elimination within 30 days. Hanum et al. [8] proposed reducing the chemotherapy dosage, increasing angiogenic dormancy, and adjusting infusion rates to manage glioma cases more effectively. Sujitha et al. [9–11] found that radiotherapy and chemotherapy combinations could reduce tumor growth and enhance glial cell proliferation. Additionally, Kaviyan et al. [12] and Sharma et al. [13] identified effective interactions between cancer cells and immunotherapy, while Ghasemabad et al. [14] demonstrated that anti–angiogenic treatments can reduce side effects and boost treatment efficacy even with patient-specific uncertainties. A more detailed version of Table 1 is available in the appendix.

In addition to the above-mentioned models, Pinho et al. [15] developed an ODE model to simulate the interactions among normal cells, vascular cancer cells, endothelial cells, a chemotherapeutic agent, and an anti–angiogenic agent during tumor growth. Their results demonstrate how anti–angiogenic therapy can enhance the effectiveness of chemotherapy in controlling tumor progression. This model has recently gained considerable attention for its ability to capture key therapeutic dynamics in vascular tumor development. Building on the work of Pinho et al., the present study seeks to advance the understanding of vascular cancer progression under therapeutic interventions, with particular focus on scenarios involving tumor regrowth. Specifically, we extend their ODE framework to a reaction–diffusion (RD) model that incorporates heterogeneous cell growth behaviors. We show that the extended model offers valuable insights into the role of spatial dynamics and therapy-induced heterogeneity in influencing treatment outcomes and the likelihood of vascular cancer relapse.

The remaining parts of this paper are organized as follows. Section 2 introduces the extended model, including its formulation and underlying assumptions. Section 3 presents a detailed analysis of the model, encompassing the existence and stability of six distinct equilibrium solutions, with explicit stability conditions derived for each case. This section also includes a global sensitivity analysis, which is critical for guiding the numerical simulations. Section 4 offers a numerical investigation of numerical bifurcations emerging from the model, explores potential scenarios of cancer relapse, and evaluates the predicted efficacy of various treatment combinations, including chemotherapy, antiangiogenic therapy, and immunotherapy. Finally, Section 5 discusses the key findings, acknowledges the study's limitations, and outlines directions for future research.

Table 1. Overview of recent modeling and simulation approaches for analyzing tumor progression and treatment efficacy.

Author, year	Key research objective and outcomes	References
De Luca et al., 2025	Analyzes the dynamics of blood vessel formation and its impact on tumor growth.	[16]
Lampropoulos et al., 2025	Evaluates treatment effects on tumor progression and vascular dynamics.	[17]
Kuznetsov et al., 2025	Suggests that the efficacy of antiangiogenic therapy depends on tumor size.	[18]
Sujitha et al., 2024	Models chemo-radiotherapy in brain tumor treatment, assessing its effectiveness in tumor reduction.	[11]
Kaviyan et al., 2023	Demonstrates therapeutic effects and interaction between cancer cells and immunotherapy.	[12]
Hernandez-Rivera, 2023	Stochastic predictive modeling of tumor growth, enhancing treatment adaptability and effectiveness.	[3]
Hanum et al., 2023	Studies impact of chemotherapy and anti–angiogenic therapy on drug resistance in glioma growth.	[8]
Sujitha et al., 2023	Combined therapy and minimal impact of time delays can improve glioma treatment.	[10]
Santurio et al., 2022	Chimeric antigen receptor T (CAR-T) cell therapy dynamics highlight on-target, off-tumor effects, particularly in neuronal loss.	[19]
Ghasemabad et al., 2022	Designs effective drug delivery in the treatment of vascular cancer tumors using a genetic algorithm tool.	[14]
Khalili et al., 2021	Studies optimal control methods for drug delivery in cancerous tumours via anti–angiogenic therapy and chemotherapy.	[20]
Sadeghi et al., 2021	Designs a fuzzy control for drug dosage delivery in cancer treatment.	[7]
El Haout et al., 2021	Compares several drug intervention strategies, including independent and combined treatments	[21]
Urenda-Cazares, 2020	Analyzes the synergistic effects of chemotherapy and oncolytic virotherapy on tumor growth.	[22]
Samanta et al., 2017	Combined or pulsed therapies improve tumor control, reduce sessions, and enhance survival.	[23]
Rodrigues et al., 2016	Examines how continuous low-dose chemotherapy can inhibit tumor growth by targeting the tumor vasculature.	[24]
Li et al., 2016[a]	Provides insights into how angiogenesis influences tumor growth and response to therapies.	[25]
Guiraldello et al., 2016[a]	Evaluates the efficacy of the maximum tolerated dose and metronomic chemotherapy strategies.	[26]
Pinho et al., 2013	Simulates tumor growth dynamics, showing how anti–angiogenic agents enhance chemotherapy's effectiveness.	[15]

Note: [a] *PDE and DDE models. All other cases proposed or used ODE models.*

2. The extended model

We consider a bounded three-dimensional spatial domain ($\Omega \subset \mathbf{R^3}$) representing vascular tumor and its adjacent tissue environment, within which transport, growth, and vascular interactions are modeled. Then the proposed model of vascular cancer dynamics is formulated by the following set of reaction–diffusion (RD) equations.

$$\frac{\partial c_1}{\partial t} = \alpha_1 c_1^{r_1}(1-c_1)^{s_1} - q_1 c_1 c_2 - p_1(c_3,\omega)\frac{c_1 y}{a_1+c_1}, \tag{2.1}$$

$$\frac{\partial c_2}{\partial t} = \alpha_2 c_2^{r_2}\left[1-\frac{c_2}{1+\gamma c_3}\right]^{s_2} - q_2 c_1 c_2 - p_2(c_3,\omega)\frac{c_2 y}{a_2+c_2} + D_2\nabla^2 c_2, \tag{2.2}$$

$$\frac{\partial c_3}{\partial t} = \alpha_3 c_3^{r_3}(1-c_3)^{s_3} + \beta c_2 - \frac{p_3 c_3 \omega}{a_3+c_3} + D_3\nabla^2 c_3, \tag{2.3}$$

$$\frac{\partial y}{\partial t} = \delta - \left[\xi + \frac{d_1 c_1}{a_1+c_1} + \frac{d_2 c_2}{a_2+c_2}\right] y + D_4\nabla^2 y, \tag{2.4}$$

$$\frac{\partial \omega}{\partial t} = \phi - \left[\eta + \frac{d_3 c_3}{a_3+c_3}\right]\omega + D_5\nabla^2\omega, \tag{2.5}$$

where the variables $c_1(\mathbf{x},t)$, $c_2(\mathbf{x},t)$, and $c_3(\mathbf{x},t)$ represent the concentrations of normal cells, cancer cells, and endothelial cells at location $\mathbf{x}$ and time $t \geq 0$ scaled by their corresponding carrying capacities, respectively. The variable $y(\mathbf{x},t)$ denotes the concentration of the chemotherapy agent, while $\omega(\mathbf{x},t)$ indicates the concentration of the anti–angiogenic agent. The first terms on the right-hand side of Eqs (2.1)–(2.3) correspond to cells' growth behaviors, which is an extended version of the standard logistic growth model [27]. Parameters r_i and s_i control the lag and stationary phase of cell growth [27]. The rest of the parameters are described in Table 2. Note that the parameters are normalized values mostly derived from Pinho's study [15]. Additionally, some of the parameters are assumed within a reasonable range to explore model behavior under varying conditions in our study in Table 2. The proposed model incorporates diffusion terms and extends the classical logistic growth model to enrich the dynamics of the model originally proposed by Pinho et al. [15].

For $i = 1, 2, 3$, according to Peleg's model [27], the parameter r_i governs exponential growth behavior, where $r_i < 1$ suppresses exponential growth, indicating a limited growth capacity, and $r_i > 1$ exceeds exponential growth. Similarly, the parameter $s_i > 1$ reflects heightened sensitivity to resource depletion, leading to population decline, while $s_i < 1$ indicates reduced sensitivity, allowing a more resilient population to stabilize near the carrying capacity.

The novelty of the model is described as follows. For Eq (2.1), the dynamics of normal cells include the modified logistic growth based on Peleg's generalized model (first term), competition with cancer cells (second term), and death induced by chemotherapy and anti–angiogenic agents (third term). Diffusion is excluded for c_1 based on the biological reasoning that normal cells often remain stationary due to strong cell adhesion, which anchors them to their environment, wereas detached normal cells typically undergo anoikis (a programmed cell death mechanism) thus eliminating the need for a diffusion term. In Eq (2.2), the first term is the modified logistic growth based on Peleg's

generalized model influenced by angiogenesis (through γc_3), experience competition with normal cells, and are targeted by chemotherapy and anti–angiogenic agents. The diffusion term $D_2\nabla^2 c_2$ captures their spatial spread due to metastatic behavior. Cancer cells $c_2(\mathbf{x}, t)$ diffuse widely due to their loss of adhesion properties, enabling them to invade tissues, enter the circulatory system, and metastasize to distant parts of the body, as described by Letellier et al. [28]. In Eq (2.3), the first term is the modified logistic growth based on Peleg's generalized model, and the second term is the endothelial cells that are stimulated by cancer cells (the term βc_2) and suppressed by anti–angiogenic agents. Their movement is modeled by diffusion $D_3\nabla^2 c_3$, representing local vascular remodeling, which represents their ability to diffuse within the body as demonstrated in Figure 3 of [29]. Diffusion terms for endothelial cells are included to model their localized movement within the tumor environment, capturing their role in forming blood vessels to support tumor growth. Equation (2.4) represents the chemotherapy agent introduced via the infusion rate δ and degraded by washout ξ and interactions with normal and cancer cells. The term inside the brackets models saturation effects via Holling-type functional responses. In Eq (2.5), the anti–angiogenic agent is infused at a rate ϕ and eliminated through washout η and uptake by endothelial cells. The variables $w(\mathbf{x}, t)$ and $y(\mathbf{x}, t)$ represent drugs within the system that are subject to diffusion due to their role in transporting therapeutic agents throughout the body.

Table 2. Description, baseline values, and range of model parameters with the references. These values are used for model simulations in Section 4.

Parameter	Description	Value	Range of values	References
α_1	NCs' proliferation rate	0.0068	$(6.8\times10^{-4},\ 0.0143)$	[15]
α_2	CCs' proliferation rate	0.01	$(1.0\times10^{-3},\ 0.0210)$	[30]
α_3	ECs' proliferation rate	0.002	$(2.0\times10^{-4},\ 0.0042)$	[31]
q_1	Competition coefficient for NCs$^{(1),(2)}$	0.00702	$(7.02\times10^{-4},\ 0.0147)$	[15]
q_2	Competition coefficient for CCs$^{(1),(2)}$	0.00071	$(7.2\times10^{-5},\ 0.0015)$	[15]
γ	Proportion of ECs$^{(2)}$ due to angiogenesis$^{(1)}$	0.1615	(0.0162, 0.3392)	[15]
β	Rate of creation of CCs due to ECs$^{(1),(2)}$	0.00371	$(3.71\times10^{-4},\ 0.0078)$	[15]
a_1	Saturation rate of the agent on NCs$^{(1),(2)}$	1.10	(0.1100, 2.3100)	[15]
a_2	Saturation rate of the agent on CCs$^{(1),(2)}$	4.6205	(0.4621, 9.7030)	[15]
a_3	Saturation rate of the agent on ECs$^{(1),(2)}$	4.6667	(0.4667, 9.7999)	[15]
d_1	Rate at which CAs$^{2)}$ combines with NCs$^{(1),(2)}$	0.0002	$(2.0\times10^{-5},\ 4.2\times10^{-4})$	[15]
d_2	Rate at which CAs$^{(2)}$ combines with CCs$^{(1),(2)}$	0.032	(0.0032, 0.0672)	[15]
d_3	Rate at which AAs combines with ECs$^{(2)}$	0.032	(0.0032, 0.0672)	[32]
p_{10}	Killing rate of CAs on NCs$^{(1),(2)}$	1.2×10^{-7}	$(1.2\times10^{-8},\ 2.52\times10^{-7})$	[15]
p_{20}	Killing rate of CAs on CCs$^{(1),(2)}$	0.2051	(0.0205, 0.4307)	[33]
p_3	Killing rate of AAs on ECs$^{(1),(2)}$	1.7143	(0.1714, 3.6000)	[15]
p_{11}	Rate of ECs' assistance of CAs for NCs$^{(1),(2)}$	4.2×10^{-8}	$(4.2\times10^{-9},\ 8.82\times10^{-8})$	[15]
p_{21}	Rate of ECs' assistance of CAs for CCs$^{(1),(2)}$	0.00431	$(4.31\times10^{-4},\ 0.0091)$	[15]
p_{12}	Rate of AAs' assistance of CAs for NCs$^{(1),(2)}$	1.0×10^{-7}	$(1.0\times10^{-8},\ 2.1\times10^{-7})$	[15]
p_{22}	Rate of AAs' assistance of CAs for CCs$^{(1),(2)}$	19.4872	(1.9487, 40.9231)	[15]
δ	Chemical infusion rate	3.3×10^{-3}	$(3.3\times10^{-4},\ 0.0069)$	[34]
ξ	Chemical washout rate	0.01813	(0.0018, 0.0381)	[35]
ϕ	Anti–angiogenic infusion rate	2.4×10^{-4}	$(2.4\times10^{-5},\ 5.04\times10^{-4})$	[34]
η	Anti–angiogenic washout rate	0.136	(0.0136, 0.2856)	[36]

Note: $^{(1)}$ *The actual parameter value has been scaled by the corresponding carrying capacity (see [15] for more details).* $^{(2)}$ *NC = normal cells $c_1(\mathbf{x}, t)$, CC = cancer cells $c_2(\mathbf{x}, t)$, EC = endothelial cell $c_3(\mathbf{x}, t)$, CA = chemotherapy agents $y(\mathbf{x}, t)$, and AA = anti–angiogenic agents $\omega(\mathbf{x}, t)$.*

In the present work, we will utilize the model for studying the simultaneous impacts of three therapies. Key model parameters representing therapeutic mechanisms include δ for chemother-

apy, ξ for anti–angiogenic therapy, and r_2 for immunotherapy. Chemotherapy targets cancer cells across all growth phases, inducing cell death and dormancy [8, 23, 34]. However, the emergence of chemotherapy-resistant cells can lead to relapse through renewed growth [2, 34, 37, 38]. Anti–angiogenic therapy delays tumor growth by inhibiting blood vessel formation, particularly in the lag and stationary phases, though tumors may adapt by revascularizing [18, 32, 39]. Immunotherapy is most effective during the exponential growth phase, targeting rapidly proliferating cancer cells with immune-recognizable markers, like PD-L1, though it may also affect healthy cells with similar markers [9, 40].

3. Model analysis

In this section, we establish the conditions for the existence and stability of equilibrium solutions.

3.1. Existence of and stability equilibria

As shown below, in the absence of diffusion, our model exhibits various types of cancer-free equilibrium (CFE) in addition to cancer-persistent equilibrium (CPE).

a. **Baseline equilibrium.** $CPE^{[0]} = (c_1^{[0]}, c_2^{[0]}, c_3^{[0]}, y^{[0]}, \omega^{[0]})$ This is the baseline equilibrium, which represents the resistance of cancer. This can happen for various reasons, such as tumor resistance [38], vascular structure [41], tumor microenvironment [42], drug delivery issues [42], or targeted therapy limitations [43].

b. **CFE Type 1.** $CPE^{[1]} = (c_1^{[1]}, 0, c_3^{[1]}, y^{[1]}, \omega^{[1]})$ This equilibrium corresponds to a cancer-free state with drugs and endothelial cells. If $p_1 = p_3 = 0$, then $c_1^{[1]} = c_3^{[1]} = 1$ and if $p_1, p_3 > 0$, then $c_1^{[1]} > 0$ and $c_3^{[1]} > 0$ exist. These are conditions for this equilibrium to exist.

c. **CFE Type 2.** $CPE^{[2]} = (c_1^{[2]}, 0, c_3^{[2]}, 0, \omega^{[2]})$ This equilibrium represents a cancer-free state with no chemotherapy agent. In this case, $c_1^{[2]} = 1$, and the equilibrium $(c_1^{[2]}, 0, c_3^{[2]}, 0, w^{[2]})$ exists if p_3 is sufficiently small.

d. **CFE Type 3.** $CPE^{[3]} = (c_1^{[3]}, 0, c_3^{[3]}, y^{[3]}, 0)$ This equilibrium represents a cancer-free state with no anti–angiogenic agent. A real positive root exists for $(c_1^{[3]}, 0, c_3^{[3]}, y^{[3]}, 0)$, provided that p_1 is sufficiently small.

e. **CFE Type 4.** $CPE^{[4]} = (c_1^{[4]}, 0, c_3^{[4]}, 0, 0)$ This equilibrium represents a cancer-free state with no drugs. If $c_2^{[4]} = y^{[4]} = w^{[4]} = 0$, then $c_1^{[4]} = c_3^{[4]} = 1$.

f. **CFE Type 5.** $CPE^{[5]} = (c_1^{[5]}, 0, 0, y^{[5]}, \omega^{[5]})$ This equilibrium corresponds to a cancer-free state with no endothelial cells. Assuming that $p_{10} = p_{12} = 0$, then $c_1^{[5]} = 1$. Thus, $(c_1^{[5]}, c_2^{[5]}, c_3^{[5]}, y^{[5]}, \omega^{[5]}) = (1, 0, 0, y^{[5]}, \frac{\phi}{\eta})$.

g. **Trivial equilibrium.** $TE = (0, 0, 0, 0, 0)$ This is the trivial equilibrium and it is biologically irrelevant. Note that TE exists only when ϕ and δ are zero, which is unrealistic.

For all types of equilibrium solutions, we will establish conditions for their stability. The Jacobian of Corollaries 1–5 are simplified versions of the Jacobian of the baseline equilibrium. Different variables have been used to represent each component of the Jacobian matrix. The specific functions

in the Jacobian have been included in the appendix.

The following theorems and corollaries address the stability of steady states in the absence of diffusion.

Theorem 1 (Stability of cancer-persistent equilibrium)**.** *The cancer-persistent equilibrium is locally asymptotically stable if the following conditions are satisfied:*
i $b_4 > 0, \quad b_3 > 0, \quad b_2 > 0, \quad b_1 > 0, \quad b_0 > 0,$
ii $b_4 b_3 b_2 > b_2^2 + b_4^2 b_1$, *and*
iii $(b_4 b_1 - b_0)(b_4 b_3 b_2 - b_2^2 - b_4^2 b_1) > b_0(b_4 b_3 - b_2)^2 + b_4 b_0^2.$

Proof. The Jacobian matrix evaluated at CPE is given by

$$J(\text{CPE}) = \begin{pmatrix} m_1 & m_2 & 0 & m_4 & m_5 \\ v_1 & v_2 & v_3 & v_4 & v_5 \\ 0 & g_2 & g_3 & 0 & g_5 \\ f_1 & f_2 & 0 & f_4 & 0 \\ 0 & 0 & z_3 & 0 & z_5 \end{pmatrix}. \tag{3.1}$$

This leads to the following characteristic polynomial:

$$\lambda^5 + b_4\lambda^4 + b_3\lambda^3 + b_2\lambda^2 + b_1\lambda + b_0 = 0 \tag{3.2}$$

$$\begin{aligned}
b_4 &= -f_4 - g_3 - m_1 - v_2 - z_5, \\
b_3 &= f_4 g_3 - f_1 m_4 + f_4 m_1 + g_3 m_1 - f_2 v_4 + f_4 v_2 - g_2 v_3 + g_3 v_2 + f_4 z_5 + g_3 z_5 - g_5 z_3 \\
&\quad + m_1 v_2 - m_2 v_1 + m_1 z_5 + v_2 z_5, \\
b_2 &= f_1 g_3 m_4 - f_4 g_3 m_1 + f_2 g_3 v_4 + f_4 g_2 v_3 - f_4 g_3 v_2 - f_4 g_3 z_5 + f_4 g_5 z_3 \\
&\quad - f_1 m_2 v_4 + f_1 m_4 v_2 + f_2 m_1 v_4 - f_2 m_4 v_1 - f_4 m_1 v_2 + f_4 m_2 v_1 \\
&\quad + g_2 m_1 v_3 - g_3 m_1 v_2 + g_3 m_2 v_1 + f_1 m_4 z_5 - f_4 m_1 z_5 - g_3 m_1 z_5 + g_5 m_1 z_3 \\
&\quad + f_2 v_4 z_5 - f_4 v_2 z_5 + g_2 v_3 z_5 - g_2 v_5 z_3 - g_3 v_2 z_5 + g_5 v_2 z_3 - m_1 v_2 z_5 + m_2 v_1 z_5, \\
b_1 &= f_1 g_2 m_4 v_3 + f_1 g_3 m_2 v_4 - f_1 g_3 m_4 v_2 - f_2 g_3 m_1 v_4 + f_2 g_3 m_4 v_1 - f_4 g_2 m_1 v_3 \\
&\quad + f_4 g_3 m_1 v_2 - f_4 g_3 m_2 v_1 - f_1 g_3 m_4 z_5 + f_1 g_5 m_4 z_3 + f_4 g_3 m_1 z_5 - f_4 g_5 m_1 z_3 \\
&\quad - f_2 g_3 v_4 z_5 + f_2 g_5 v_4 z_3 - f_4 g_2 v_3 z_5 + f_4 g_2 v_5 z_3 + f_4 g_3 v_2 z_5 - f_4 g_5 v_2 z_3 \\
&\quad + f_1 m_2 v_4 z_5 - f_1 m_4 v_2 z_5 - f_2 m_1 v_4 z_5 + f_2 m_4 v_1 z_5 + f_4 m_1 v_2 z_5 - f_4 m_2 v_1 z_5 \\
&\quad - g_2 m_1 v_3 z_5 + g_2 m_1 v_5 z_3 - g_2 m_5 v_1 z_3 + g_3 m_1 v_2 z_5 - g_3 m_2 v_1 z_5 - g_5 m_1 v_2 z_3 + g_5 m_2 v_1 z_3, \\
b_0 &= f_1 g_2 m_4 v_5 z_3 - f_1 g_2 m_4 v_3 z_5 - f_1 g_2 m_5 v_4 z_3 - f_1 g_3 m_2 v_4 z_5 + f_1 g_3 m_4 v_2 z_5 \\
&\quad + f_1 g_5 m_2 v_4 z_3 - f_1 g_5 m_4 v_2 z_3 + f_2 g_3 m_1 v_4 z_5 - f_2 g_3 m_4 v_1 z_5 - f_2 g_5 m_1 v_4 z_3 \\
&\quad + f_2 g_5 m_4 v_1 z_3 + f_4 g_2 m_1 v_3 z_5 - f_4 g_2 m_1 v_5 z_3 + f_4 g_2 m_5 v_1 z_3 - f_4 g_3 m_1 v_2 z_5 \\
&\quad + f_4 g_3 m_2 v_1 z_5 + f_4 g_5 m_1 v_2 z_3 - f_4 g_5 m_2 v_1 z_3.
\end{aligned}$$

By the Routh–Hurwitz criterion, the CPE is locally asymptotically stable. This completes the proof.

Remark 1. *The stability conditions outlined in Theorem 3.1 are sensitive to the values of system parameters. It is worth noting that the violation of these conditions can occur in multiple, non-unique ways. In particular, the inequalities specified in the theorem can be violated through a variety of parameter combinations, all of which may result in a loss of stability of the steady states. This underscores the importance of a thorough parameter sensitivity analysis when applying these results.*

We have the following corollaries.

Corollary 1 (Stability of CFE Type 1 equilibrium)**.** *Let $p_1 > 0$ and $p_3 > 0$. Assume that*

(H_1) $a_3 = 0$ and $d_1 = 0$,

(H_2) $(m_1 + v_2) < 0$, and

(H_3) $(m_1 v_2 - m_2 v_1) > 0$.

Then the cancer-free equilibrium (Type 1) $CPE^{[1]} = (c_1^{[1]}, 0, c_3^{[1]}, y^{[1]}, \omega^{[1]})$ is locally asymptotically stable.

Proof. It can be shown that $c_1^{[1]} > 0$ and $c_3^{[1]} > 0$, provided $p_1, p_3 > 0$, and the Jacobian matrix, evaluated at the CFE Type 1 is given by

$$J(CPE^{[1]}) = \begin{pmatrix} m_1 & m_2 & 0 & m_4 & m_5 \\ v_1 & v_2 & 0 & 0 & 0 \\ 0 & g_2 & g_3 & 0 & g_5 \\ f_1 & 0 & 0 & f_4 & 0 \\ 0 & 0 & z_3 & 0 & z_5 \end{pmatrix}. \tag{3.3}$$

Also (H_1) guarantees that $y^{[1]} > 0$ and $\omega^{[1]} > 0$. Hence, $CPE^{[1]} = (c_1^{[1]}, 0, c_3^{[1]}, y^{[1]}, \omega^{[1]})$ exists. The Jacobian matrix $J(CPE^{[1]})$ in (3.3) has the following characteristic polynomial.

$$z_3\Big(f_1 g_5 m_4 (v_2 - \lambda) - (f_4 - \lambda)(g_2 m_5 v_1 + g_5 (m_1 - \lambda)(v_2 - \lambda) - g_5 m_2 v_1)\Big) \\ + (g_3 - \lambda)(z_5 - \lambda)\Big(f_1 m_4 (\lambda - v_2) + (f_4 - \lambda)((m_1 - \lambda)(v_2 - \lambda) - m_2 v_1)\Big)$$

Under Hypothesis 1 (H_1), where $a_3 = 0$ and $d_1 = 0$, we have $f_1 = 0$ and $z_3 = 0$. Substituting these into the characteristic polynomial gives rise to

$$(g_3 - \lambda)(z_5 - \lambda)(f_4 - \lambda)\left((m_1 - \lambda)(v_2 - \lambda) - m_2 v_1\right).$$

There are five eigenvalues as follows:

$\lambda_1 = g_3$

$\lambda_2 = z_5$

$\lambda_3 = f_4$

The remaining two eigenvalues are the roots of the following quadratic polynomial:

$$\lambda^2 - (m_1 + v_2)\lambda + (m_1 v_2 - m_2 v_1).$$

As shown in Section B of the appendix, $g_3 < 0$, $z_5 < 0$, and $f_4 < 0$. Hence, the first three eigenvalues are negative.

For the quadratic part, we have

$$\lambda^2 - (m_1 + v_2)\lambda + (m_1 v_2 - m_2 v_1),$$

the roots have negative real parts under assumptions (H_2) and (H_3).

Thus, under the conditions specified in H_1, H_2, and H_3, all eigenvalues have negative real parts, and the cancer-free equilibrium (Type 1) is locally asymptotically stable.

Corollary 2 (Stability of CFE Type 2)**.** *The cancer-free equilibrium (Type 2) exists if* $c_1^{[2]} = 1$ *and if* p_3 *is sufficiently small. Moreover, this equilibrium is locally asymptotically stable if the following conditions are satisfied:*

(i) $q_4 > 0, \quad q_3 > 0, \quad q_2 > 0, \quad q_1 > 0, \quad q_0 > 0;$

(ii) $q_4 q_3 q_2 > q_2^2 + q_4^2 q_1;$

(iii) $(q_4 q_1 - q_0)(q_4 q_3 q_2 - q_2^2 - q_4^2 q_1) > q_0(q_4 q_3 - q_2)^2 + q_4 q_0^2.$

Proof. The existence of $CPE^{[2]} = (c_1^{[2]}, 0, c_3^{[2]}, 0, \omega^{[2]})$ is guaranteed since $c_1^{[2]} = 1$ and p_3 is sufficiently small, leading to positive components of $CPE^{[2]}$. The Jacobian matrix evaluated at the CFE Type 2 is given by

$$J(CPE^{[2]}) = \begin{pmatrix} m_1 & m_2 & 0 & m_4 & 0 \\ v_1 & v_2 & 0 & 0 & 0 \\ 0 & g_2 & g_3 & 0 & g_5 \\ 0 & 0 & 0 & f_4 & 0 \\ 0 & 0 & z_3 & 0 & z_5 \end{pmatrix} \tag{3.4}$$

The characteristic polynomial from the Jacobian matrix is given as

$$\lambda^5 + q_4\lambda^4 + q_3\lambda^3 + q_2\lambda^2 + q_1\lambda + q_0 = 0$$

where the coefficients are

$$\begin{aligned}
q_4 &= f_4 + g_3 + m_1 + v_2 + z_5, \\
q_3 &= -\left(f_4 g_3 + f_4 m_1 + f_4 v_2 + f_4 z_5 + g_3 m_1 + g_3 v_2 + g_3 z_5 - g_5 z_3 + m_1 v_2 + m_1 z_5 - m_2 v_1 + v_2 z_5\right), \\
q_2 &= f_4 g_3 m_1 + f_4 g_3 v_2 + f_4 g_3 z_5 - f_4 g_5 z_3 + f_4 m_1 v_2 + f_4 m_1 z_5 - f_4 m_2 v_1 + f_4 v_2 z_5 \\
&\quad + g_3 m_1 v_2 + g_3 m_1 z_5 - g_3 m_2 v_1 + g_3 v_2 z_5 - g_5 m_1 z_3 - g_5 v_2 z_3 + m_1 v_2 z_5 - m_2 v_1 z_5, \\
q_1 &= -\left(f_4 g_3 m_1 v_2 + f_4 g_3 m_1 z_5 - f_4 g_3 m_2 v_1 + f_4 g_3 v_2 z_5 - f_4 g_5 m_1 z_3 - f_4 g_5 v_2 z_3\right. \\
&\quad \left. + f_4 m_1 v_2 z_5 - f_4 m_2 v_1 z_5 + g_2 m_5 v_1 z_3 - g_3 m_1 v_2 z_5 + g_3 m_2 v_1 z_5 + g_5 m_1 v_2 z_3 - g_5 m_2 v_1 z_3\right), \\
q_0 &= -f_4 g_2 m_5 v_1 z_3 + f_4 g_3 m_1 v_2 z_5 - f_4 g_3 m_2 v_1 z_5 - f_4 g_5 m_1 v_2 z_3 + f_4 g_5 m_2 v_1 z_3.
\end{aligned}$$

By the Routh–Hurwitz criterion, the CFE Type 2 is locally asymptotically stable.

Corollary 3 (Stability of CFE Type 3)**.** *The cancer-free equilibrium (Type 3) exists if p_1 is sufficiently small, and it is locally asymptotically stable if these conditions are satisfied:*

(i) $t_1 > 0$*;*

(ii) $t_3 > 0$*;*

(iii) $t_1 t_2 > t_3$*,*

where

$$\begin{aligned} t_1 &= -(m_1 + v_2 + f_4) \\ t_2 &= -\left(f_1 m_4 - m_1 v_2 - f_4 m_1 - f_4 v_2 + m_2 v_1\right) \\ t_3 &= f_1 m_4 v_2 - f_4 m_1 v_2 + f_4 m_2 v_1. \end{aligned}$$

Proof. The Jacobian matrix evaluated at the CFE Type 3 is a simplified version of (6)

$$J(CPE^{[3]}) = \begin{pmatrix} m_1 & m_2 & 0 & m_4 & m_5 \\ v_1 & v_2 & 0 & 0 & 0 \\ 0 & g_2 & g_3 & 0 & g_5 \\ f_1 & 0 & 0 & f_4 & 0 \\ 0 & 0 & 0 & 0 & z_5 \end{pmatrix} \tag{3.5}$$

The characteristic polynomial is given by

$$(g_3 - \lambda)(z_5 - \lambda)\left(f_1 m_4(\lambda - v_2) + (f_4 - \lambda)\left((m_1 - \lambda)(v_2 - \lambda) - m_2 v_1\right)\right)$$

As shown in Section B of the appendix, the first two eigenvalues are negative:

$$\lambda_1 = g_3$$

$$\lambda_2 = z_5$$

This reduces the polynomial to

$$\left(f_1 m_4(\lambda - v_2) + (f_4 - \lambda)\left((m_1 - \lambda)(v_2 - \lambda) - m_2 v_1\right)\right),$$

which is simplifies to

$$\begin{aligned} &- \lambda^3 \\ &+ (m_1 + v_2 + f_4)\lambda^2 \\ &+ \left(f_1 m_4 - m_1 v_2 - f_4 m_1 - f_4 v_2 + m_2 v_1\right)\lambda \\ &+ \left(-f_1 m_4 v_2 + f_4 m_1 v_2 - f_4 m_2 v_1\right) \end{aligned}$$

Thus, the cubic characteristic polynomial becomes

$$-\lambda^3 + (m_1 + v_2 + f_4)\lambda^2 + \left(f_1 m_4 - m_1 v_2 - f_4 m_1 - f_4 v_2 + m_2 v_1\right)\lambda + \left(-f_1 m_4 v_2 + f_4 m_1 v_2 - f_4 m_2 v_1\right)$$

Multiplying through by -1 for the standard form, we have

$$\lambda^3 + t_1\lambda^2 + t_2\lambda + t_3 = 0$$

By the Routh–Hurwitz criterion, the CPE Type 3 is locally asymptotically stable under Assumptions *(i), (ii),* and *(iii)*.

Corollary 4 (Stability of CFE Type 4)**.** *The cancer-free equilibrium (Type 4) is locally asymptotically stable if the following conditions are satisfied:*

(i) $v_2 < 0$ *and*

(ii) $m_2 v_1 < 0$.

Proof. Note that $c_2^{[4]} = y^{[4]} = w^{[4]} = 0$, which implies $c_1^{[4]} = c_3^{[4]} = 1$. Hence, the Jacobian matrix evaluated at the $CPE^{[4]} = (c_1^{[4]}, 0, c_3^{[4]}, 0, 0)$ is given by

$$J(CPE^{[4]}) = \begin{pmatrix} 0 & m_2 & 0 & m_4 & 0 \\ v_1 & v_2 & 0 & 0 & 0 \\ 0 & g_2 & 0 & 0 & g_5 \\ 0 & 0 & 0 & f_4 & 0 \\ 0 & 0 & 0 & 0 & z_5 \end{pmatrix} \tag{3.6}$$

The characteristic polynomial is given by

$$(f_4 - \lambda)(z_5 - \lambda)(v_2\lambda^2 - \lambda^3 + m_2 v_1 \lambda)$$

As shown in Section B of the appendix, the first two eigenvalues are negative:

$\lambda_1 = f_4$

$\lambda_2 = z_5$

The remaining cubic polynomial is given by

$$\lambda^3 - v_2\lambda^2 - m_2 v_1 \lambda$$

By the Routh–Hurwitz criterion the CPE Type 4 is locally asymptotically stable.

Corollary 5 (Stability of CFE Type 5)**.** *The cancer-free equilibrium (Type 5) is locally asymptotically stable if the following conditions are satisfied:*

(i) $b_4 > 0, \quad b_3 > 0, \quad b_2 > 0, \quad b_1 > 0, \quad b_0 > 0;$

(ii) $b_4 b_3 b_2 > b_2^2 + b_4^2 b_1;$

(iii) $(b_4 b_1 - b_0)(b_4 b_3 b_2 - b_2^2 - b_4^2 b_1) > b_0(b_4 b_3 - b_2)^2 + b_4 b_0^2.$

Proof. Assuming $p_{10} = p_{12} = 0$, then $c_1^{[5]} = 1$. Thus, $(c_1^{[5]}, c_2^{[5]}, c_3^{[5]}, y^{[5]}, \omega^{[5]}) = (1, 0, 0, y^{[5]}, \frac{\phi}{\eta})$ with $y^{[5]} > 0$. The Jacobian matrix evaluated at the CFE Type 5 is given by

$$J(CPE^{[5]}) = \begin{pmatrix} m_1 & m_2 & 0 & m_4 & m_5 \\ v_1 & v_2 & 0 & 0 & 0 \\ 0 & g_2 & g_3 & 0 & 0 \\ f_1 & 0 & 0 & f_4 & 0 \\ 0 & 0 & z_3 & 0 & z_5 \end{pmatrix} \tag{3.7}$$

The coefficients of the characteristic polynomial are

$$
\begin{aligned}
b_4 &= -f_4 - g_3 - m_1 - v_2 - z_5,\\
b_3 &= f_4g_3 - f_1m_4 + f_4m_1 + g_3m_1 + f_4v_2 + g_3v_2 + f_4z_5 + g_3z_5\\
&\quad + m_1v_2 - m_2v_1 + m_1z_5 + v_2z_5,\\
b_2 &= f_1g_3m_4 - f_4g_3m_1 - f_4g_3v_2 - f_4g_3z_5 + f_1m_4v_2 - f_4m_1v_2\\
&\quad + f_4m_2v_1 - g_3m_1v_2 + g_3m_2v_1 + f_1m_4z_5 - f_4m_1z_5 - g_3m_1z_5\\
&\quad - f_4v_2z_5 - g_3v_2z_5 - m_1v_2z_5 + m_2v_1z_5,\\
b_1 &= f_4g_3m_1v_2 - f_1g_3m_4v_2 - f_4g_3m_2v_1 - f_1g_3m_4z_5 + f_4g_3m_1z_5\\
&\quad + f_4g_3v_2z_5 - f_1m_4v_2z_5 + f_4m_1v_2z_5 - f_4m_2v_1z_5\\
&\quad - g_2m_5v_1z_3 + g_3m_1v_2z_5 - g_3m_2v_1z_5,\\
b_0 &= f_1g_3m_4v_2z_5 + f_4g_2m_5v_1z_3 - f_4g_3m_1v_2z_5 + f_4g_3m_2v_1z_5.
\end{aligned}
$$

Now using the Routh–Hurwitz criterion given in the hypotheses of the corollary, the CFE Type 5 is locally asymptotically stable.

3.2. Stability analysis in the presence of diffusion

In this section, we perform an analytical investigation of the full reaction–diffusion model to assess its potential for diffusion-driven instability, commonly known as Turing pattern formation. We denote the cancer-persistent equilibrium by $\mathrm{CPE}^{[0]}$ both in the absence and presence of diffusion. This is justified because the equilibrium point arises from solving the steady-state condition, which is independent of the diffusion terms. That is, diffusion affects the dynamics but not the location of the spatially homogeneous steady state.

We consider the general form of the reaction–diffusion system as follows:

$$\frac{\partial \mathbf{u}}{\partial t} = \mathbf{F}(\mathbf{u}) + D\nabla^2\mathbf{u},$$

where $\mathbf{u} = (c_1, c_2, c_3, y, \omega)^\top$ is the vector of model variables, and $D = \mathrm{diag}(0, D_2, D_3, D_4, D_5)$ is the diagonal matrix of diffusion coefficients. The function $\mathbf{F}(\mathbf{u})$ encodes the nonlinear reaction kinetics.

We linearize the system around the spatially homogeneous steady state

$$\mathrm{CPE}^{[0]} = \left(c_1^{[0]}, c_2^{[0]}, c_3^{[0]}, y^{[0]}, \omega^{[0]}\right)$$

by introducing small perturbations of the form

$$\mathbf{u}(x,t) = \mathbf{u}^* + \epsilon\mathbf{W}_k e^{\lambda t}\cos(kx),$$

where $\epsilon \ll 1$ and k is the spatial wavenumber. Substituting into the PDE system and linearizing yields the eigenvalue problem:

$$\lambda\mathbf{W}_k = (J - k^2D)\mathbf{W}_k,$$

where J is the Jacobian matrix evaluated at $\mathbf{u}^* = \mathrm{CPE}^{[0]}$ and $J_k := J - k^2D$ is the diffusion-modified Jacobian.

The Jacobian matrix ($CPE^{[0]}$) takes the form

$$J = \begin{pmatrix} m_1 & m_2 & 0 & m_4 & m_5 \\ v_1 & v_2 & v_3 & v_4 & v_5 \\ 0 & g_2 & g_3 & 0 & g_5 \\ f_1 & f_2 & 0 & f_4 & 0 \\ 0 & 0 & z_3 & 0 & z_5 \end{pmatrix}$$

and the diffusion-modified Jacobian becomes

$$J_k = J - k^2 D = \begin{pmatrix} m_1 & m_2 & 0 & m_4 & m_5 \\ v_1 & v_2 - D_2k^2 & v_3 & v_4 & v_5 \\ 0 & g_2 & g_3 - D_3k^2 & 0 & g_5 \\ f_1 & f_2 & 0 & f_4 - D_4k^2 & 0 \\ 0 & 0 & z_3 & 0 & z_5 - D_5k^2 \end{pmatrix}. \tag{3.8}$$

The characteristic polynomial of J_k is given by

$$\det(\lambda I - J_k) = \lambda^5 + b_4^{[k]}\lambda^4 + b_3^{[k]}\lambda^3 + b_2^{[k]}\lambda^2 + b_1^{[k]}\lambda + b_0^{[k]} = 0,$$

where the coefficients $b_i^{[k]}$ depend smoothly on the diffusion terms and can be written as

$$b_i^{[k]} = b_i + D_i k^2,$$

with $D_i k^2 \geq 0$, $i = 0, 1, 2, 3, 4$, $D_0 = 0$, and b_i as defined in the non–diffusive case.

Solving the characteristic equation yields the dispersion relation $\lambda(k)$, which determines the growth or decay of perturbations with the spatial wavenumber k. The linear stability is determined by the sign of $\mathrm{Re}[\lambda(k)]$ as follows:

(a) If $\mathrm{Re}[\lambda(k)] < 0$ for all $k \geq 0$, the system is linearly stable.

(b) If $\mathrm{Re}[\lambda(k)] > 0$ for some $k > 0$, then the system is unstable to spatial perturbations and may exhibit Turing instability.

Building on the stability results established in Section 3.1, we demonstrate that diffusion-driven instability does not occur in our setting. On the contrary, diffusion exhibits a stabilizing effect, thereby reinforcing the validity of the stability results in the presence of diffusion.

Theorem 2 (Stability of $\mathrm{CPE}^{[0]}$ with diffusion)**.** *Assume that the non–diffusive equilibrium is locally asymptotically stable; that is, the original coefficients b_4, b_3, b_2, b_1, b_0 satisfy the following Routh–Hurwitz conditions:*

(i) $b_4 > 0, \quad b_3 > 0, \quad b_2 > 0, \quad b_1 > 0, \quad b_0 > 0;$

(ii) $b_4 b_3 b_2 > b_2^2 + b_4^2 b_1;$

(iii) $(b_4 b_1 - b_0)(b_4 b_3 b_2 - b_2^2 - b_4^2 b_1) > b_0(b_4 b_3 - b_2)^2 + b_4 b_0^2.$

Then for all $k \in \mathbb{R}$, the diffusion-modified equilibrium CPE$^{[0]}$ remains locally asymptotically stable. That is, all eigenvalues λ of J_k have negative real parts.

Proof. Let $b_i^{[k]} = b_i + D_i k^2$ for $i = 0, 1, 2, 3, 4$, where each $D_i k^2 \geq 0$ represents the contribution from diffusion. Since the first variable does not diffuse, we set $D_0 k^2 = 0$. We have

$$
\begin{aligned}
b_4 &= -f_4 - g_3 - m_1 - v_2 - z_5,\\
b_3 &= f_4 g_3 - f_1 m_4 + f_4 m_1 + g_3 m_1 - f_2 v_4 + f_4 v_2 - g_2 v_3 + g_3 v_2 + f_4 z_5 + g_3 z_5 - g_5 z_3\\
&\quad + m_1 v_2 - m_2 v_1 + m_1 z_5 + v_2 z_5,\\
b_2 &= f_1 g_3 m_4 - f_4 g_3 m_1 + f_2 g_3 v_4 + f_4 g_2 v_3 - f_4 g_3 v_2 - f_4 g_3 z_5 + f_4 g_5 z_3\\
&\quad - f_1 m_2 v_4 + f_1 m_4 v_2 + f_2 m_1 v_4 - f_2 m_4 v_1 - f_4 m_1 v_2 + f_4 m_2 v_1\\
&\quad + g_2 m_1 v_3 - g_3 m_1 v_2 + g_3 m_2 v_1 + f_1 m_4 z_5 - f_4 m_1 z_5 - g_3 m_1 z_5 + g_5 m_1 z_3\\
&\quad + f_2 v_4 z_5 - f_4 v_2 z_5 + g_2 v_3 z_5 - g_2 v_5 z_3 - g_3 v_2 z_5 + g_5 v_2 z_3 - m_1 v_2 z_5 + m_2 v_1 z_5,\\
b_1 &= f_1 g_2 m_4 v_3 + f_1 g_3 m_2 v_4 - f_1 g_3 m_4 v_2 - f_2 g_3 m_1 v_4 + f_2 g_3 m_4 v_1 - f_4 g_2 m_1 v_3\\
&\quad + f_4 g_3 m_1 v_2 - f_4 g_3 m_2 v_1 - f_1 g_3 m_4 z_5 + f_1 g_5 m_4 z_3 + f_4 g_3 m_1 z_5 - f_4 g_5 m_1 z_3\\
&\quad - f_2 g_3 v_4 z_5 + f_2 g_5 v_4 z_3 - f_4 g_2 v_3 z_5 + f_4 g_2 v_5 z_3 + f_4 g_3 v_2 z_5 - f_4 g_5 v_2 z_3\\
&\quad + f_1 m_2 v_4 z_5 - f_1 m_4 v_2 z_5 - f_2 m_1 v_4 z_5 + f_2 m_4 v_1 z_5 + f_4 m_1 v_2 z_5 - f_4 m_2 v_1 z_5\\
&\quad - g_2 m_1 v_3 z_5 + g_2 m_1 v_5 z_3 - g_2 m_5 v_1 z_3 + g_3 m_1 v_2 z_5 - g_3 m_2 v_1 z_5 - g_5 m_1 v_2 z_3 + g_5 m_2 v_1 z_3,\\
b_0 &= f_1 g_2 m_4 v_5 z_3 - f_1 g_2 m_4 v_3 z_5 - f_1 g_2 m_5 v_4 z_3 - f_1 g_3 m_2 v_4 z_5 + f_1 g_3 m_4 v_2 z_5\\
&\quad + f_1 g_5 m_2 v_4 z_3 - f_1 g_5 m_4 v_2 z_3 + f_2 g_3 m_1 v_4 z_5 - f_2 g_3 m_4 v_1 z_5 - f_2 g_5 m_1 v_4 z_3\\
&\quad + f_2 g_5 m_4 v_1 z_3 + f_4 g_2 m_1 v_3 z_5 - f_4 g_2 m_1 v_5 z_3 + f_4 g_2 m_5 v_1 z_3 - f_4 g_3 m_1 v_2 z_5\\
&\quad + f_4 g_3 m_2 v_1 z_5 + f_4 g_5 m_1 v_2 z_3 - f_4 g_5 m_2 v_1 z_3.
\end{aligned}
$$

Given that all baseline coefficients $b_i > 0$ by assumption, it follows that $b_i^{[k]} > 0$ for all $k \geq 0$. Therefore, the first Routh–Hurwitz condition (i) remains satisfied in the presence of diffusion. The Routh–Hurwitz conditions (ii) and (iii) depend continuously on the coefficients $b_i^{[k]}$, which increase monotonically with k^2 due to the non-negative diffusion contributions $D_i k^2 \geq 0$. Since b_i satisfy these inequalities, the added diffusion terms strengthen them.

Hence, the Routh–Hurwitz conditions remain satisfied for all $k \geq 0$. Consequently, all eigenvalues of the characteristic polynomial remain negative, ensuring stability.

This result rules out the possibility of diffusion-driven (Turing-type) instability near the cancer-persistent equilibrium. The stability analysis of the cancer-free equilibrium with the presence of diffusion can be found in Section E of the appendix.

3.3. Global sensitivity analysis of the model

Given the importance of the parameters r_i and s_i in stability and numerical bifurcation analyses of the model, we first investigated the effects of these parameters. Figure 1(a) shows that increasing the value of r_i delays the divergence from the unstable trivial steady state, whereas increasing the value of s_i delays the convergence to the stable positive steady state. Hence, r_i and s_i can define numerical

bifurcation thresholds, which will be numerically investigated in the next section. Due to the computational burden of including all combinations of the logistic exponents r_i and s_i in the global sensitivity analysis, we assumed these exponents to be equal to 1, reducing the model to Pinho's formulation [15]. This allowed for a tractable sensitivity analysis focused on other parameters. To compensate, we subsequently performed a dedicated numerical bifurcation analysis to investigate the effects of varying the logistic exponents, thereby complementing the sensitivity findings (see Section 4.1).

To assess the influence of the model's parameters (other than r_i and s_i) on the stable cancer-free state, we conducted a global sensitivity analysis (GSA) using the classification and regression tree (CRT) method. The analysis identified key independent variables contributing to the classification of the cancer-free state and provided insights into their relative importance. The CRT-based classification model demonstrated an overall predictive accuracy of 77.5%, with higher accuracy for the "No" class (80.4%) compared with the "Yes" class (66.9%). This suggests that while the model effectively identifies cases with an unstable cancer-free state, it has moderate performance in classifying cases that are stable. The cross-validation risk estimate (0.448 ± 0.003) closely aligns with the resubstitution estimate (0.440 ± 0.003), indicating a valid model performance. Furthermore, the resulting classification tree contained 63 nodes, with 32 terminal nodes and a maximum depth of 5. The inclusion of 24 independent variables in the final model suggests that multiple interacting parameters contribute to the stable cancer-free state. The model structure, combined with the parameters' importance ranking, provides insights into which biological and treatment-related factors significantly affect long-term remission outcomes.

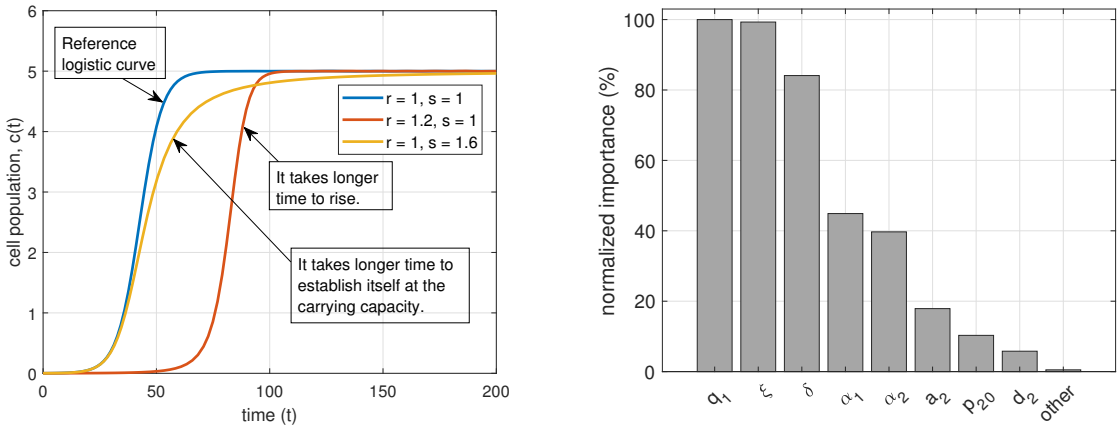

(a) Extended logistic growth model behaviors.

(b) Importance of model parameters.

Figure 1. Effects of model parameters. (a) The lag and stationary phases of cell growth are increased with larger values of r and s, respectively. (b) Bar chart of normalized model importance. Parameters with less than 5% importance are combined into "Other".

Figure 1(b) provides the bar chart of the normalized importance of model parameters. It can be seen that the top three parameters influencing the stability of the cancer-free steady state are the competition coefficient q_1 for normal cells (NCs), the chemical washout rate ξ, and the chemical infusion rate δ. These parameters play a critical role in determining whether the system maintains a healthy equilibrium or transitions toward a cancer-dominated state. The high sensitivity to these parameters suggests that

therapeutic strategies aimed at modulating chemical exposure and enhancing the competitive advantage of NCs could be effective in sustaining remission and preventing relapse. The lower-ranked variables, while included in the model, contribute minimally to classification, suggesting possible redundancy or secondary effects in the system's dynamics.

4. Numerical simulations

4.1. Numerical bifurcation analysis

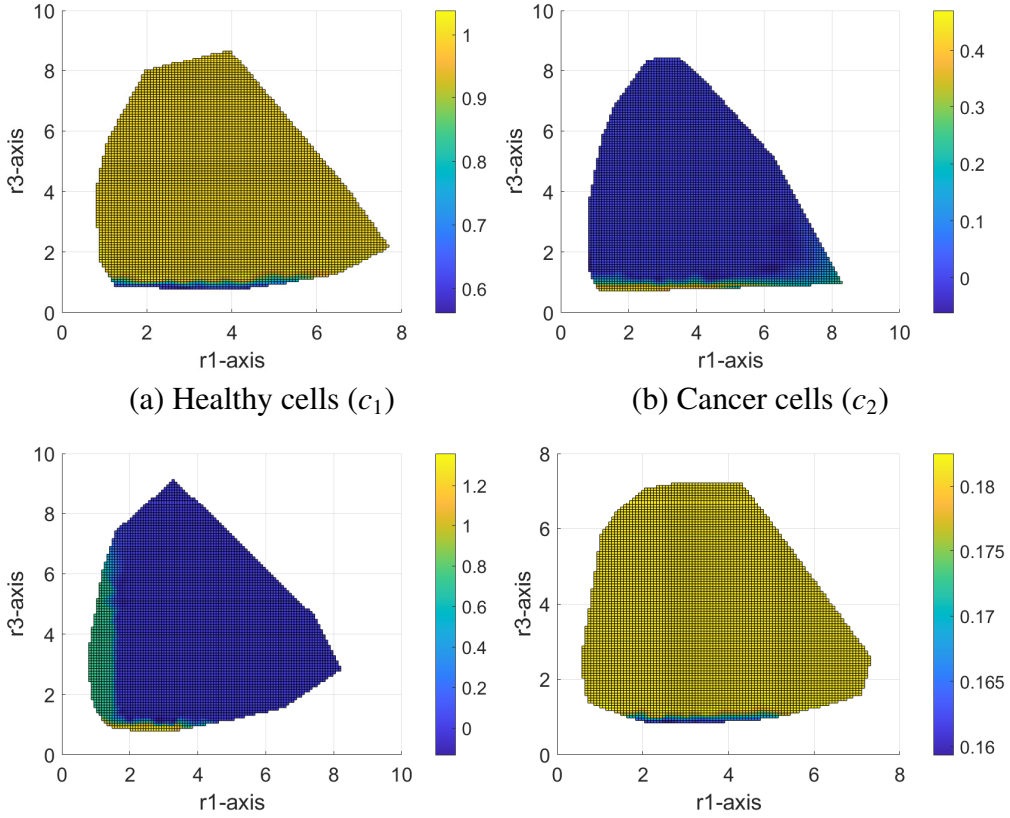

(a) Healthy cells (c_1) (b) Cancer cells (c_2)

(c) Endothelial cells (c_3) (d) Chemotherapy agent (y)

Figure 2. Bifurcation simulations when $r_1 > 1$ and $r_3 > 1$ but $s_1 = s_3 = 1$. (a) Increasing r_3 significantly boosts healthy cell growth. The density of healthy cells increases when r_3 exceeds values near 1. When r_1 exceeds a critical value near 6, then the diagram will be independent of r_3 values. The reverse of (a) happens in (b): when r_3 is greater than 1 and $r_1 > 6$, the cancer cells die. However, (c) shows that higher cancer densities lead to increased immune response, but there is no significant impact on chemotherapy and anti–angiogenic concentration when r_1 and r_3 are increased. A fifth panel for anti–angiogenic concentration was not included because it is almost identical to the fourth panel.

In this section, we investigate the influence of the parameters r_i and s_i in shaping the tumor growth dynamics. We examine the effects of how different values of the parameters r_i and s_i on the healthy and cancer cell populations at the stable steady states. In Case 1, where r_1 and r_3 are greater than 1,

increasing r_3 significantly enhances healthy cell growth, especially when $r_1 > 6$, also leading to the decline of cancer cells (see Figure 2). This bifurcation behavior aligns with biological mechanisms targeted by therapies that prolong the cancer cells' lag phase by inducing cell cycle arrest [44, 45]. Similarly, increasing s_3 also promotes healthy cell growth (see Figure 3), though its effects are less pronounced than those of r_3. This is a good addition to the bifurcation diagrams by Pinho et al., since different values for r and s were not previously explored.

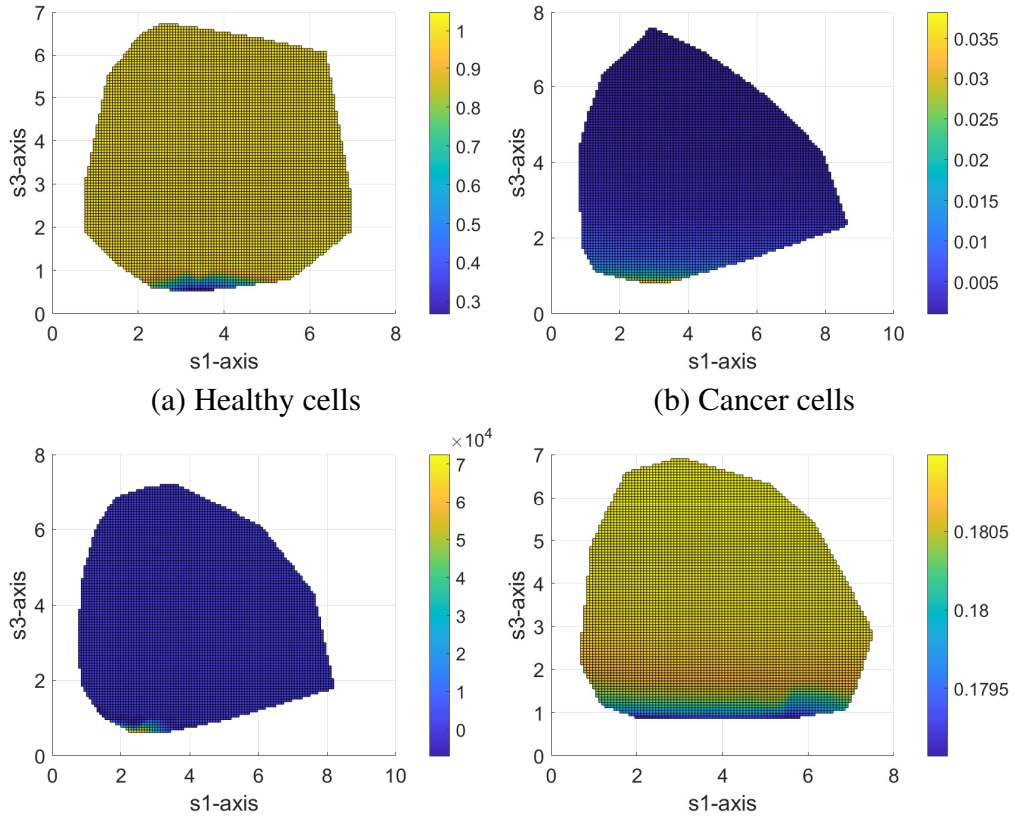

(a) Healthy cells (b) Cancer cells

(c) Endothelial cells (d) Chemotherapy agent

Figure 3. Bifurcation simulations when s_1 and $s_3 > 1$ but $r_1 = r_3 = 1$. Increasing s_3 significantly boosts healthy cells' growth. Healthy cells increase when $s_3 > 0.4$ and $s_1 > 4$. The reverse of (a) happens in (b) the r_1 and r_3 combination is more effective in cancer cells' death. Part (c) shows that higher cancer densities lead to an increased immune response, but there is no significant impact on chemotherapy and anti–angiogenic concentration when s_1 and s_3 are increased. A fifth panel for anti–angiogenic concentration was not included because it is almost identical to the fourth panel.

We also find that maintaining $r_1 < 2$ is essential for preventing healthy cells' collapse, while $r_2 > 1$ is effective in suppressing cancer cell proliferation when $r_1 > 4.6$. The effect of $r_2 > 1$ justifies why $r_2 > 1$ enables the therapies to be more effective, especially anti–angiogenic therapy and immunotherapy. These results are illustrated through numerical bifurcation diagrams provided in Section C of the appendix (Figures A1 and A2). Finally, comparing the influence of the parameter r- and s, we find that the parameter r exhibit a stronger capacity to destabilize the cancer-dominated steady state and pro-

mote healthy cells' recovery, while increased cancer cell densities generally elevate immune responses without significantly affecting the chemotherapy concentration.

4.2. *Cancer relapse*

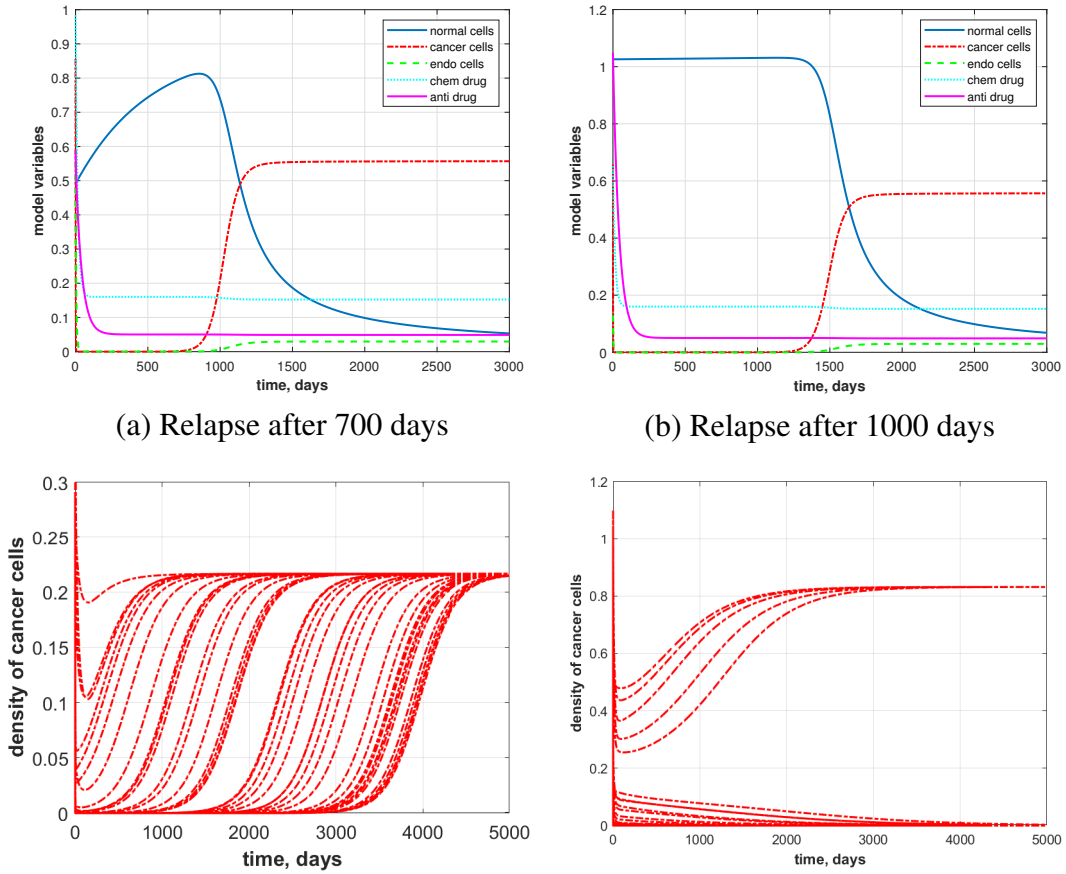

(a) Relapse after 700 days

(b) Relapse after 1000 days

(c) Relapse at different times

(d) Bistability of relapse and cure

Figure 4. Relapse analysis for the cases $r = 2$ and $s = 1$. (a) and (b) Relapse after 700 and 1000 days, respectively; (c) relapse due to partial cancer treatment; (d) bistable equilibrium solutions lead to relapse or successful treatment, depending on the initial cancer cell densities.

Using Matlab ODE and PDE solvers, we numerically explored the possibility of cancer relapse based on the parameters from Pinho's paper and the range of values presented in Table 2. Figure 4 demonstrates the dynamics of cancer relapse in the absence of diffusion. Panels (a) and (b) show relapse scenarios in which the tumor re-emerges after extended periods (700 and 1000 days). In contrast, Panels (c) and (d) show bistable tumor dynamics, emphasizing the system's sensitivity to the initial conditions and treatment parameters. Using Matlab pdepe solver, we numerically investigated the solutions of the reaction–diffusion model under Dirichlet boundary conditions and various sets of parameter values. Figure 5 illustrates the progression of cancer relapse at two different time points. Panel (a) shows a moderate tumor size after 50 days, while Panel (b) indicates significant tumor regrowth after 200 days, highlighting the long-term potential for relapse.

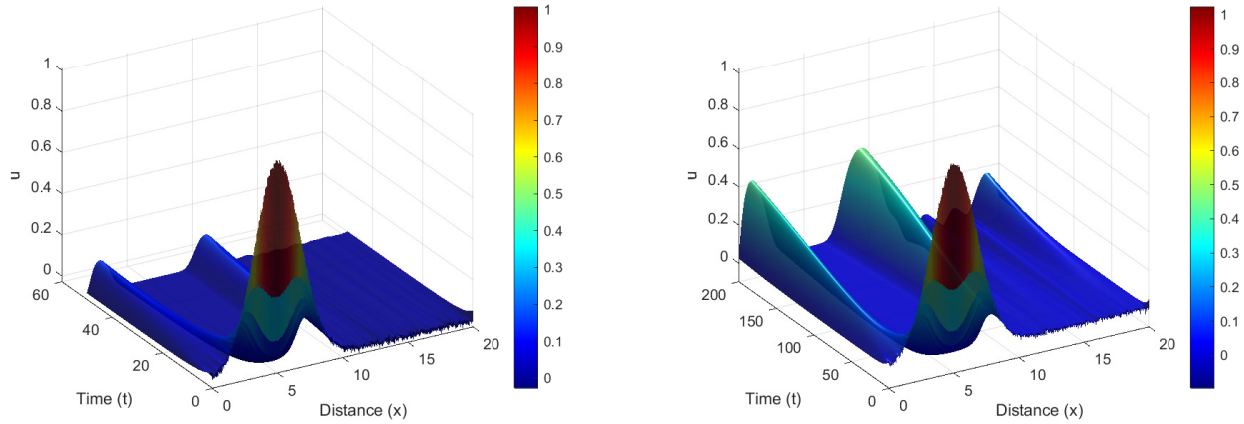

(a) After 50 days (b) After 200 days

Figure 5. Numerical simulations of the reaction–diffusion (RD) model indicate that cancer relapse may occur in tissues or organs that previously exhibited no detectable tumor growth but are located in close proximity to the primary tumor site.

4.3. Predicted efficacy of treatments

A general overview of vascular cancer progression and corresponding treatments synthesized from the existing literature and medical sources is shown in Table 3. The classification of vascular cancer stages is based on tumor size, progressing from smaller (0.8 inches) to larger tumors (2 inches or more). Treatment strategies evolve accordingly, beginning with chemotherapy for smaller tumors and advancing to a combination of chemotherapy, anti–angiogenic therapy, and immunotherapy for more advanced stages. This classification acknowledges the complex nature of vascular cancers, where treatment approaches must be adapted according to tumor progression and individual patient responses.

Table 3. Summary of vascular cancer stages, associated therapies, and the corresponding tumor sizes and treatment durations used in model simulations.

Stage	Tumor size and treatment duration	Types of therapy	References
Stage I	< 2 cm (0.8 inches); 4–6 weeks	Adjuvant chemotherapy	[46, 47]
Stage II	2–5 cm (0.8–2 inches); 6–8 weeks	Chemotherapy	[46]
Stage III	> 5 cm (2 inches); 3–6 months	Chemotherapy and anti–angiogenic therapy	[46]
Stage IV	Tumor size widely varies; ongoing treatment lasting months to years	Chemotherapy and anti–angiogenic therapy, and immunotherapy,	[48, 49]

As shown in Figure 6, at Stage 1, with a tumor size less than 2 cm, chemotherapy alone was effective in significantly reducing tumor volume over a 50-day period. Without chemotherapy, the tumor exhibited substantial 38% tumor growth in the same time frame. At Stage 2, with tumor sizes ranging between 3 and 5 cm, chemotherapy continued to demonstrate effectiveness, achieving successful tumor reduction in 60 days. However, without chemotherapy, the tumor size increased by approximately

30%. As tumors exceed 5 cm in Stage 3, simulations of the RD model showed that a combination of chemotherapy and anti–angiogenic therapy led to full tumor regression within 110 days, highlighting the potency of this dual approach at advanced stages (see Figure 7). When chemotherapy was administered without anti–angiogenic therapy, a reduction was observed initially, but the tumor size plateaued after 160 days. In cases where only anti–angiogenic therapy was applied without chemotherapy, the tumor grew by 209%, showing the importance of chemotherapy as a primary treatment agent in cancer treatment. Without any therapeutic intervention, the tumor size increased drastically by 421%, which is consistent with expected rapid tumor growth at this advanced stage.

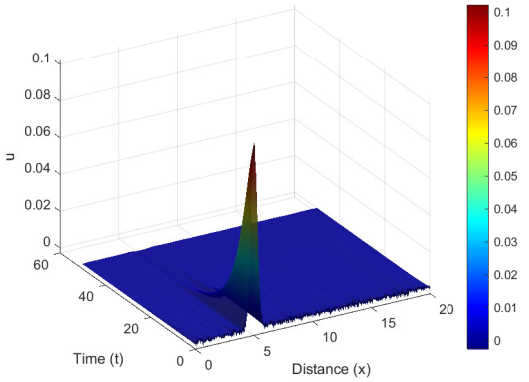

(a) Stage 1 with chemotherapy

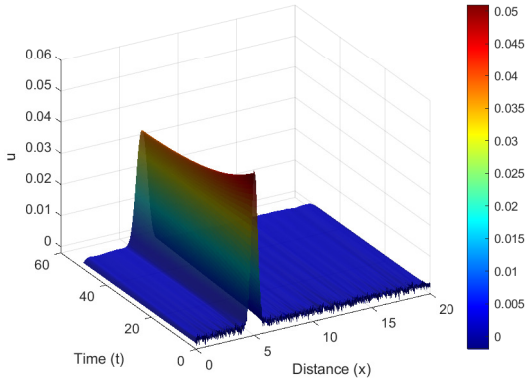

(b) Stage 1 without chemotherapy

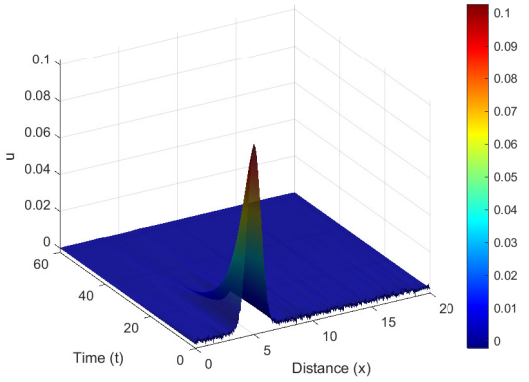

(c) Stage 2 with chemotherapy

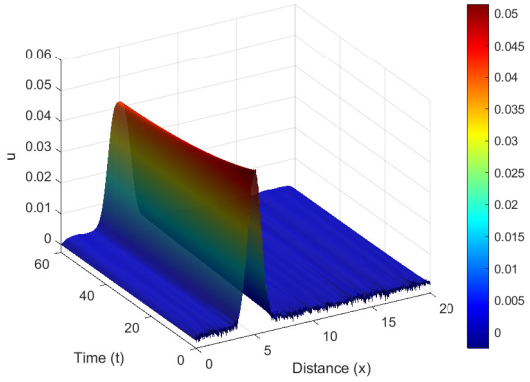

(d) Stage 2 without chemotherapy

Figure 6. The tumor size dynamics in Stages 1 and 2, with or without chemotherapy. For Stage 1, (a) chemotherapy results in a significant 94% reduction in tumor size over a 50-day period; (b) without chemotherapy, the tumor growth increases by approximately 38%. Panels (c) and (d) show similar results for Stage 2 with chemotherapy. There is a 97% reduction in tumor size after 60 days in (c) and in (d) without chemotherapy, and there is a 30% increase in tumor area.

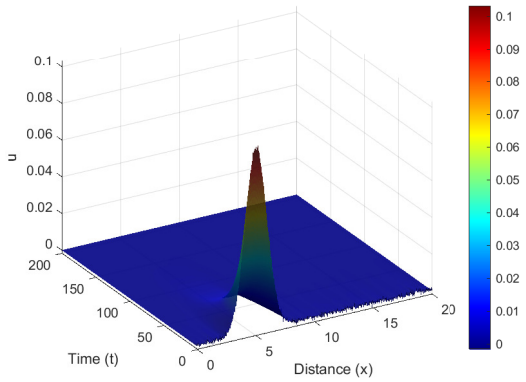

(a) Chemotherapy and anti-angiogenic therapy

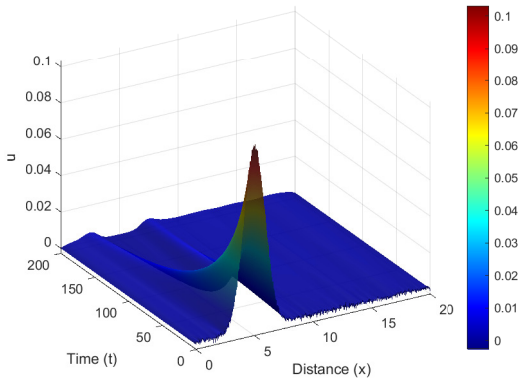

(b) Chemotherapy only

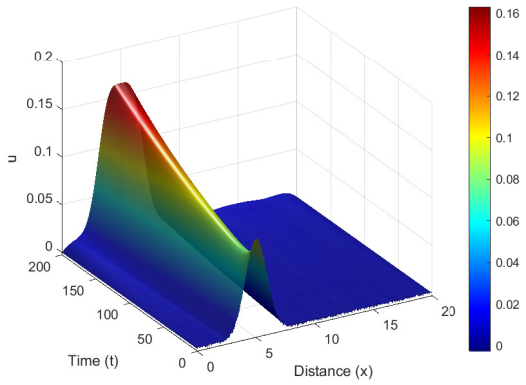

(c) Anti–angiogenic therapy only

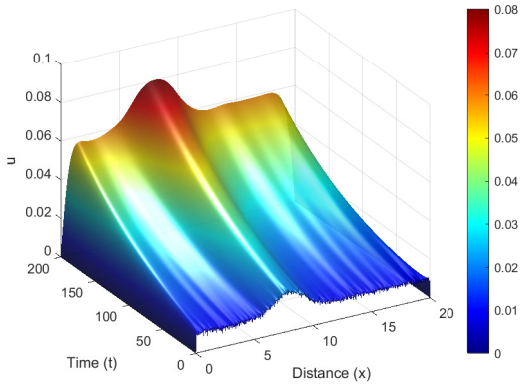

(d) No intervention

Figure 7. Predicted outcomes of chemotherapy and anti–angiogenic therapy on tumor growth in Stage 3, where tumor size is greater than 5 cm over a 200-day period. (a) The combination of chemotherapy and anti–angiogenic therapy results in nearly a 100% reduction in tumor size after 150 days. (b) Chemotherapy alone reduces the tumor area by 84% after 200 days; (c) anti–angiogenic therapy alone is not effective and leads to a 209% increase in tumor size; (d) in the absence of both therapies, the tumor size increases by 421%, demonstrating the rapid progression of cancer without any intervention.

In Stage 4, where tumor size varies widely, the combination of chemotherapy, immunotherapy, and anti–angiogenic therapy proved to be the most effective, achieving full tumor reduction in approximately 200 days (see Figure 8). When chemotherapy was excluded and both immunotherapy and anti–angiogenic therapy were retained, tumor size reduced by 76% over a span of 730 days. Comparatively, chemotherapy combined with immunotherapy without anti–angiogenic therapy led to an 84% reduction, while the pairing of chemotherapy and anti–angiogenic therapy excluding immunotherapy achieved an 87% reduction. In the absence of any intervention, tumor growth was excessive, reflecting the expected aggressive nature of untreated Stage 4 cancer (see Figure A3).

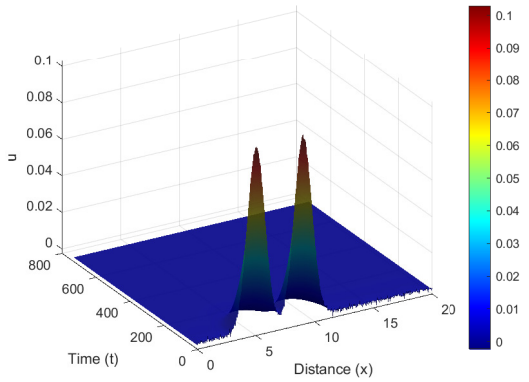

(a) Chemotherapy, immunotherapy and anti–angiogenic therapy

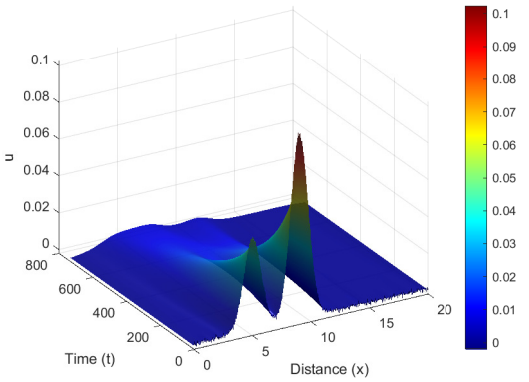

(b) Anti–angiogenic therapy and immunotherapy

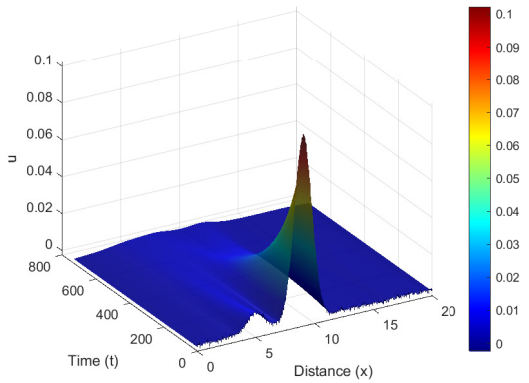

(c) Chemotherapy and immunotherapy

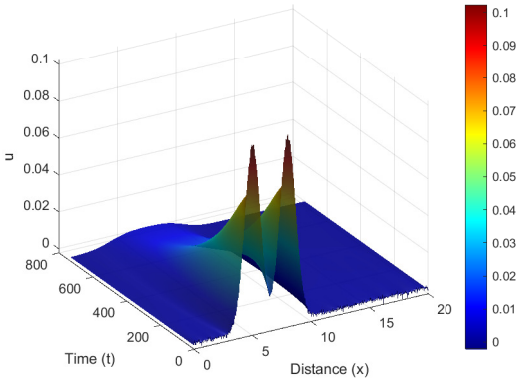

(d) Chemotherapy and anti–angiogenic therapy

Figure 8. Tumor response to combined therapies in Stage 4 cancer. (a) Combined effect of chemotherapy, immunotherapy, and anti–angiogenic therapy, resulting in complete tumor regression within 200 days; (b) predicted outcome when chemotherapy is absent, leading to a 76% decrease in tumor size; (c) the effect of chemotherapy and immunotherapy without anti–angiogenic therapy, resulting in 84% tumor size reduction; (d) the combination of chemotherapy and anti–angiogenic therapy, without immunotherapy, leading to a 87% reduction in tumor size.

We also computed the mean areas under the curve (AUC) for each cancer stage, providing a detailed view of the therapy's effectiveness over time. Figure 9 illustrates the impact of chemotherapy and anti–angiogenic therapy on tumor progression across different cancer stages. In both Stage 1 and Stage 2, the presence of chemotherapy significantly reduces tumor area, while its absence leads to tumor growth. The advanced stage results further emphasize that combined chemotherapy and anti–angiogenic therapy lead to complete tumor regression, whereas the absence of one or both therapies results in substantial tumor growth. A summary of these findings is presented in Table 4. For additional details, please see Table A2 in section D of the appendix.

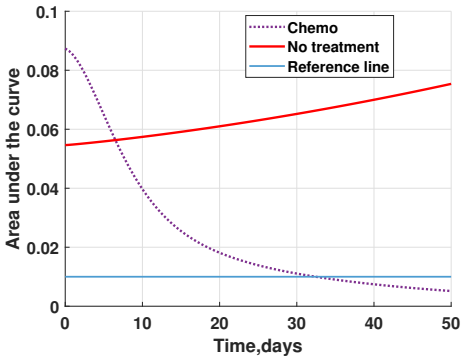

(a) AUC for Stage 1

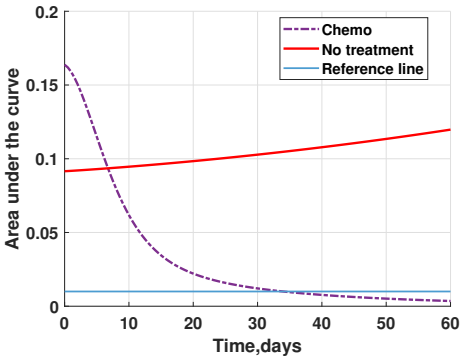

(b) AUC for Stage 2

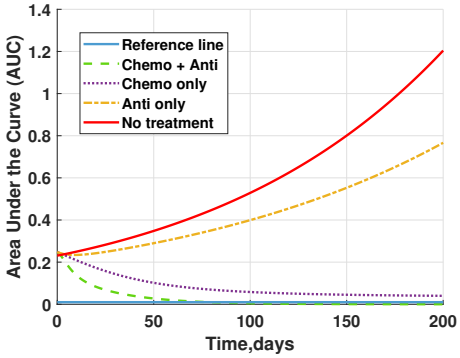

(c) AUC for Stage 3

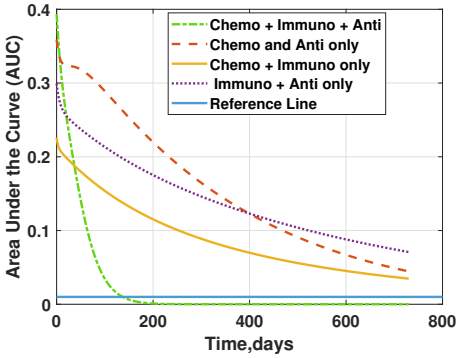

(d) AUC for Stage 4

Figure 9. Area under the curve (AUC) plots showing changes to tumor volume across different stages and treatments. Panels (a) and (b) show Stages 1 and 2: Chemotherapy reduces tumor area by 94% and 97%, while the absence of treatment leads to tumor growth. Panel (c) highlights the critical role of chemotherapy and anti–angiogenic therapy in Stage 3, with untreated cases showing up to a 421% increase in tumor size. Panel (d) shows how effective chemotherapy, immunotherapy, and anti–angiogenic therapy are in cancer treatment in Stage 4.

Table 4. Predicted efficacy of cancer therapies across different stages of vascular cancer. The associated model parameters are shown in parentheses. Mean AUC values, tumor volumes before and after treatment, and volume reductions (as percentages) are shown.

Stage, Treatment (Parameters)	Pretreatment	Post-treatment
Stage I: Chemotherapy (δ)	AUC = 0.0874, V = 0.0194 cm^3	AUC = 0.0052, V = 0.0003 cm^3 (–94.1%)
Stage II: Chemotherapy (δ)	AUC = 0.1634, V = 0.0499 cm^3	AUC = 0.004, V = 10^{-6}cm^3 (–97.8%)
Stage III: Chemotherapy (δ) and anti–angiogenic (ξ)	AUC = 0.2472 V = 0.092 cm^3	AUC=0.0001, V = 10^{-6} cm^3 (–99.9%)
Stage IV: Chemotherapy (δ), anti–angiogenic (ξ), and immunotherapy (r_2)	AUC = 0.3931, V = 0.1858 cm^3	AUC = 10^{-6}, V = 10^{-6} cm^3 (–99.9%)

5. Discussion

This study represents a further advancement in cancer modeling aimed at measuring the efficacy of various therapies across different stages of vascular cancer. The numerical bifurcation analysis in this study revealed that increasing the parameter r significantly boosts healthy cells' growth and can lead to eradication of cancer cells when exceeding critical values. The cell growth dynamics were not captured by Pinho's model because the parameters r and s were restricted to 1. The modified logistic growth model based on Peleg's generalized model gave better insights into how changes in the parameter values for r and s give another perspective on the cell growth dynamics. The extended model, through both simulation and analytical results, corroborates the findings of Pinho et al. [15], while offering additional insights into the effectiveness of various interventions when implemented individually or in combination. The simulation results in Section 4.3 emphasize the paramount importance of chemotherapy, particularly when combined with anti–angiogenic therapy and immunotherapy, in effectively managing tumor growth across various cancer stages. The assessment of the different stages of cancer is based on the simulations of the RD model and the specific parameters of this paper. These results suggest that treatment efficacy varies significantly across different stages of cancer. Early-stage tumors respond well to chemotherapy alone, whereas advanced tumors benefit the most from combination therapies. However, the effectiveness of these treatments is highly dependent on the specific parameters used in the simulations.

Dirichlet boundary conditions were used in the simulations to represent fixed concentrations of cell populations and therapeutic agents at the boundary, simulating the presence of a constant microenvironment or external regulation at the tumor's margin [50–52]. To assess the sensitivity of the model to boundary conditions, we also conducted simulations using no-flux Neumann boundary conditions for selected cases. While Neumann conditions are often considered to be more biologically realistic, particularly in enclosed tissue environments, we observed that the overall dynamics of the system remained largely consistent across both boundary condition types. This robustness can be attributed to the sufficiently large spatial domain used in the model, which minimizes the influence of boundary effects on interior behavior. These findings suggest that the key qualitative behaviors of the system are not significantly dependent on the specific choice of boundary conditions, supporting the broader applicability of our results. Beyond the current model, the literature supports the evolution of cancer models toward greater biological realism [53, 54]. For instance, advanced ODE-based models incorporate drug pharmacokinetics, tumor shrinkage rate constants, and immune-cancer interactions (e.g., cytotoxic T lymphocytes dynamics during immunotherapy) [55]. Moreover, emerging approaches using fractional calculus have gained traction due to their ability to capture memory effects and anomalous diffusion behaviors, offering improved fidelity in simulating tumor growth and treatment response [56–58]. In particular, the work by Unni and Seshaiyer [59] demonstrates the impact of immune system components such as natural killer cells, dendritic cells, and CD8+ cytotoxic T cells in modulating tumor dynamics, providing further motivation for integrative modeling that accounts for complex biological feedback mechanisms.

Some limitations of are study is that we do not specifically define parameter ranges or offer thorough biological explanations for the stability conditions determined using the Routh–Hurwitz criteria in the explorations of stability in Section 3.1. This restricts the results' direct relevance to particular

tumor situations. This is due to the complexity of the Jacobian matrix and the associated characteristic polynomials. Furthermore, even though our model incorporates some spatial components through reaction–diffusion terms, we have not conducted a thorough analytical analysis of how spatial patterns like wavefronts or instabilities originate. In order to improve the model's mathematical and biological insight, future research will concentrate on determining the analytical circumstances under which such spatial patterns might emerge. As part of our future research direction, we intend to calibrate and validate the model using available patient-derived datasets due to the in silico nature of our findings.

In conclusion, by examining the dynamic interplay between healthy and cancerous cells under various therapeutic regimes, the extended model offers insights for the design of personalized, stage-specific cancer treatments.

Use of AI tools declaration

In the creation of this paper, Grammarly was used to check for spelling errors.

Acknowledgments

This work was supported by the University of Missouri—Kansas City (UMKC) Funding for Excellence Program (2024–2025). Any opinions, findings, conclusions, or recommendations expressed in this material are those of the authors and do not necessarily reflect the views of the university.

Conflict of interest

All authors declare no conflicts of interest in this paper.

References

1. K. E. de Visser, J. A. Joyce, The evolving tumor microenvironment: From cancer initiation to metastatic outgrowth, *Cancer Cell*, **41** (2023), 424–446. https://doi.org/10.1016/j.ccell.2023.02.016
2. T. Azizi, Mathematical modelling of cancer treatments, resistance, optimization, *AppliedMath*, **5** (2025), 40. https://doi.org/10.3390/appliedmath5020040
3. A. Hernández-Rivera, P. Velarde, A. Zafra-Cabeza, J. M. Maestre, A stochastic model predictive control approach to deal with cancerous tumor growth, in *2023 9th International Conference on Control, Decision and Information Technologies (CoDIT)*, IEEE, (2023), 2037–2042. https://doi.org/10.1109/CoDIT58514.2023.10284136
4. C. Antonescu, Malignant vascular tumors—An update, *Mod. Pathol.*, **27** (2014), S30–S38. https://doi.org/10.1038/modpathol.2013.171
5. T. A. Partanen, K. Paavonen, Lymphatic versus blood vascular endothelial growth factors and receptors in humans, *Microsc. Res. Tech.*, **55** (2001), 108–121. https://doi.org/10.1002/jemt.1174
6. X. Shi, X. Wang, W. Yao, D. Shi, X. Shao, Z. Lu, et al., Mechanism insights and therapeutic intervention of tumor metastasis: Latest developments and perspectives, *Cell. Mol. Life Sci.*, **9** (2024), 192. https://doi.org/10.1007/s00018-024-05267-w

7. E. Sadeghi, I. Zamani, Z. G. Zarandi, S. T. Afshari, Finite-time fuzzy control design for drug dosage delivery in cancer treatment, in *2021 7th International Conference on Control, Instrumentation and Automation (ICCIA)*, IEEE, (2021), 1–6. https://doi.org/10.1109/ICCIA52082.2021.9403530
8. L. Hanum, N. Susyanto, D. Ertiningsih, Mathematical model of the impact of chemotherapy and anti-angiogenic therapy on drug resistance in glioma growth, *Comput. Math. Biophys.*, **13** (2023), 20250022. https://doi.org/10.1515/cmb-2025-0022
9. S. Sujitha, T. Jayakumar, D. Maheskumar, E. V. Kaviyan, Mathematical model of brain tumor with radiotherapy treatment, *Commun. Math. Appl.*, **14** (2023), 1039–1050. https://doi.org/10.26713/cma.v14i2.2442
10. S. Sujitha, T. Jayakumar, D. Maheskumar, Fractional model of brain tumor with chemo-radiotherapy treatment, *J. Appl. Math. Comput.*, **69** (2023), 3793–3818. https://doi.org/10.1007/s12190-023-01935-6
11. S. Sujitha, T. Jayakumar, D. Maheskumar, E. V. Kaviyan, An analytical and numerical approach to chemo-radiotherapy model for the treatment of brain tumor, *OPSEARCH*, **2024** (2024), 1–26. https://doi.org/10.1007/s12597-024-00670-9
12. E. V. Kaviyan, T. Jayakumar, S. Sujitha, D. Maheskumar, Analytical and numerical solutions for glial cells interactions between immunotherapy and cancer cells, *Commun. Math. Appl.*, **14** (2023), 925–935. https://doi.org/10.26713/cma.v14i2.2465
13. S. Sharma, G. P. Samanta, Dynamical behaviour of a tumor-immune system with chemotherapy and optimal control, *J. Nonlinear Dyn.*, **2013** (2013), 608598. https://doi.org/10.1155/2013/608598
14. E. S. Ghasemabad, I. Zamani, H. Tourajizadeh, M. Mirhadi, Z. G. Zarandi, Design and implementation of an adaptive fuzzy sliding mode controller for drug delivery in treatment of vascular cancer tumours and its optimisation using genetic algorithm tool, *IET Syst. Biol.*, **16** (2022), 345–355. https://doi.org/10.1049/syb2.12051
15. S. T. R. Pinho, F. S. Bacelar, R. F. S. Andrade, H. I. Freedman, A mathematical model for the effect of anti-angiogenic therapy in the treatment of cancer tumours by chemotherapy, *Nonlinear Anal. Real World Appl.*, **14** (2013), 815–828. https://doi.org/10.1016/j.nonrwa.2012.07.022
16. P. De Luca, A. Galletti, G. Giunta, L. Marcellino, A numerical approach for a 1D tumor-angiogenesis simulations model, *Appl. Numer. Math.*, **210** (2025), 83–94. https://doi.org/10.1016/j.apnum.2024.11.017
17. I. Lampropoulos, M. Koutsi, M. E. Kavousanakis, Modeling of chemo-radiotherapy targeting growing vascular tumors: A continuum-level approach, *PLoS One*, **20** (2025), e0301657. https://doi.org/10.1371/journal.pone.0301657
18. M. Kuznetsov, A. Kolobov, Antiangiogenic therapy efficacy can be tumor-size dependent, as mathematical modeling suggests, *Mathematics*, **12** (2024), 353. https://doi.org/10.3390/math12020353
19. D. S. Santurio, L. R. C. Barros, A mathematical model for on-target off-tumor effect of CAR-T cells on gliomas, *Front. Syst. Biol.*, **2** (2022), 923085. https://doi.org/10.3389/fsysb.2022.923085

20. P. Khalili, S. Zolatash, R. Vatankhah, S. Taghvaei, Optimal control methods for drug delivery in cancerous tumour by anti-angiogenic therapy and chemotherapy, *IET Syst. Biol.*, **15** (2021), 13–24. https://doi.org/10.1049/syb2.12010
21. S. E. Haout, M. Fatani, N. A. Farha, N. AlSawaftah, M. Mortula, G. A. Husseini, Modeling the effects of chemotherapy and immunotherapy on tumor growth, *J. Biomed. Nanotechnol.*, **17** (2021), 2505–2518. https://doi.org/10.1166/jbn.2021.3214
22. E. Urenda-Cázares, A. Gallegos, J. E. Macías-Díaz, A mathematical model that combines chemotherapy and oncolytic virotherapy as an alternative treatment against a glioma, *J. Math. Chem.*, **58** (2020), 544–554. https://doi.org/10.1007/s10910-019-01070-8
23. G. P. Samanta, R. G. Aíza, S. Sharma, Analysis of a mathematical model of periodically pulsed chemotherapy treatment, *Int. J. Dyn. Control*, **5** (2017), 842–857. https://doi.org/10.1007/s40435-015-0204-2
24. D. S. Rodrigues, P. F. A. Mancera, S. T. R. Pinho, Understanding the antiangiogenic effect of metronomic chemotherapy through a simple mathematical model, *Physica A*, **464** (2016), 251–266. https://doi.org/10.1016/j.physa.2016.07.027
25. D. Li, W. Ma, S. Guo, Stability of a mathematical model of tumour-induced angiogenesis, *Nonlinear Anal. Model. Control*, **21** (2016), 325–344. https://doi.org/10.15388/NA.2016.3.3
26. R. T. Guiraldello, M. L. Martins, P. F. A. Mancera, Evaluating the efficacies of maximum tolerated dose and metronomic chemotherapies: A mathematical approach, *Math. Biosci.*, **275** (2016), 19–26. https://doi.org/10.1016/j.mbs.2016.03.004
27. M. Peleg, M. G. Corradini, M. D. Normand, The logistic (Verhulst) model for sigmoid microbial growth curves revisited, *Food Res. Int.*, **40** (2007), 808–818. https://doi.org/10.1016/j.foodres.2007.01.012
28. C. Letellier, S. K. Sasmal, C. Draghi, F. Denis, D. Ghosh, A chemotherapy combined with an anti-angiogenic drug applied to a cancer model including angiogenesis, *Chaos Solitons Fractals*, **104** (2017), 252–263. https://doi.org/10.1016/j.chaos.2017.04.013
29. D. A. Hormuth, C. M. Phillips, C. Wu, E. A. Lima, G. Lorenzo, P. K. Jha, et al., Biologically-based mathematical modeling of tumor vasculature and angiogenesis via time-resolved imaging data, *Cancers*, **13** (2021), 3008. https://doi.org/10.3390/cancers13123008
30. J. S. Spratt, J. A. Meyer, Rates of growth of human neoplasms: part II, *J. Surg. Oncol.*, **61** (1996), 68–83. https://doi.org/10.1002/1096-9098(199601)61:1<68::AID-JSO2930610102>3.0.CO;2-E
31. B. Alberts, A. Johnson, J. Lewis, M. Raff, K. Roberts, P. Walter, *Molecular Biology of the Cell*, Taylor & Francis Books, 2002.
32. D. Hanahan, J. Folkman, Patterns and emerging mechanisms of the angiogenic switch during tumourigenesis, *Cell*, **86** (1996), 353–364. https://doi.org/10.1016/S0092-8674(00)80108-7
33. R. T. Silver, R. D. Lauper, C. I. Jarowski, *A Synopsis of Cancer Chemotherapy*, Yorke Medical Books, 1987.
34. T. Browder, C. E. Butterfield, B. M. Kraling, B. Shi, B. Marshall, M. S. O'Reilly, et al., Antiangiogenic scheduling of chemotherapy improves efficacy against experimental drug-resistant cancer, *Cancer Res.*, **60** (2001), 1878–1886.

35. R. Said, M. Abdel-Rehim, B. Sadeghia, S. Al-Hashemi, Z. Hassana, M. Hassan, Cyclophosphamide pharmacokinetics in mice: A comparison between retro orbital sampling versus serial tail vein bleeding, *Open Pharmacol. J.*, **1** (2007), 30–35. https://doi.org/10.2174/1874143600701010030

36. S. Shusterman, S. A. Grupp, R. Barr, D. Carpentieri, H. Zhao, J. M. Maris, The angiogenesis inhibitor TNP-470 effectively inhibits human neuroblastoma xenograft growth especially in the setting of subclinical disease, *Clin. Cancer Res.*, **7** (2001), 977–984.

37. J. Trobia, K. Tian, A. M. Batista, C. Grebogi, H. P. Ren, M. S. Santos, et al., Mathematical model of brain tumour growth with drug resistance, preprint, arXiv:2012.08252.

38. J. Rieth, S. Subramanian, Mechanisms of intrinsic tumor resistance to immunotherapy, *Int. J. Mol. Sci.*, **19** (2018), 1340. https://doi.org/10.3390/ijms19051340

39. S. Yonucu, D. Yilmaz, C. Phipps, M. B. Unlu, M. Kohandel, Quantifying the effects of antiangiogenic and chemotherapy drug combinations on drug delivery and treatment efficacy, *PLoS Comput. Biol.*, **13** (2017), e1005724. https://doi.org/10.1371/journal.pcbi.1005724

40. X. Shi, X. He, X. Ou, Model of tumor growth and treatment with anti-angiogenesis therapy and immunotherapy, in *2015 4th International Conference on Computer Science and Network Technology (ICCSNT)*, IEEE, (2015), 62–66. https://doi.org/10.1109/ICCSNT.2015.7491025

41. M. K. Pugsley, R. Tabrizchi, The vascular system: An overview of structure and function, *J. Pharmacol. Toxicol. Methods*, **44** (2000), 333–340. https://doi.org/10.1016/S1056-8719(00)00125-8

42. O. Trédan, C. M. Galmarini, K. Patel, I. F. Tannock, Drug resistance and the solid tumor microenvironment, *J. Natl. Cancer Inst.*, **99** (2007), 1441–1454. https://doi.org/10.1093/jnci/djm135

43. R. A. Stahel, S. Peters, *Successes and Limitations of Targeted Cancer Therapy*, Karger Medical and Scientific Publishers, 2014. https://doi.org/10.1159/isbn.978-3-318-02542-2

44. M. Broecker-Preuss, S. Müller, M. Britten, K. Worm, K. W. Schmid, K. Mann, et al., Sorafenib inhibits intracellular signaling pathways and induces cell cycle arrest and cell death in thyroid carcinoma cells irrespective of histological origin or BRAF mutational status, *BMC Cancer*, **15** (2015), 1–13. https://doi.org/10.1186/s12885-015-1186-0

45. Y. Zhang, G. Li, X. Liu, Y. Song, J. Xie, G. Li, et al., Sorafenib inhibited cell growth through the MEK/ERK signaling pathway in acute promyelocytic leukemia cells, *Oncol. Lett.*, **15** (2018), 5620–5626. https://doi.org/10.3892/ol.2018.8010

46. D. Morgensztern, S. Waqar, J. Subramanian, F. Gao, K. Trinkaus, R. Govindan, Prognostic significance of tumor size in patients with Stage III non–small-cell lung cancer: A surveillance, epidemiology, and end results (SEER) survey from 1998 to 2003, *J. Thorac. Oncol.*, **7** (2012), 1479–1484. https://doi.org/10.1097/JTO.0b013e318267d032

47. E. F. Patz Jr, S. Rossi, D. H. Harpole Jr, J. E. Herndon, P. C. Goodman, Correlation of tumor size and survival in patients with Stage IA non-small cell lung cancer, *Chest*, **117** (2000), 1568–1571. https://doi.org/10.1378/chest.117.6.1568

48. F. Yang, H. Chen, J. Xiang, Y. Zhang, J. Zhou, H. Hu, et al., Relationship between tumor size and disease stage in non-small cell lung cancer, *BMC Cancer*, **10** (2010), 474. https://doi.org/10.1186/1471-2407-10-474

49. P. Ciciola, P. Cascetta, C. Bianco, L. Formisano, R. Bianco, Combining immune checkpoint inhibitors with anti-angiogenic agents, *J. Clin. Med.*, **9** (2020), 873. https://doi.org/10.3390/jcm9030675

50. A. Andreozzi, M. Iasiello, P. A. Netti, The effects of exterior boundary conditions on a internally heated tumor tissue with a thermoporoelastic model, *J. Biomech.*, **113** (2020), 110122. https://doi.org/10.1016/j.jbiomech.2020.110122

51. Y. Zhuang, S. Cui, Analysis of a free boundary problem modeling the growth of spherically symmetric tumors with angiogenesis, *Acta Appl. Math.*, **161** (2019), 153–169. https://doi.org/10.1007/s10440-019-00236-w

52. J. Wang, H. Zheng, Y. Jia, H. K. Xu, Spatial patterns and bifurcation analysis of a diffusive tumour-immune model, *Taiwanese J. Math.*, **25** (2021), 553–577. https://doi.org/10.11650/tjm/200904

53. K. K. Menta, M. Bani-Yaghoub, B. B. C. Youan, Uncovering dual oscillatory regimes in p53-mdm2 dynamics: A data-driven modeling approach with implications for cancer progression, *BioSystems*, **2025** (2025), 105540. https://doi.org/10.1016/j.biosystems.2025.105540

54. M. Bani-Yaghoub, D. E. Amundsen, Turing-type instabilities in a mathematical model of notch and retinoic acid pathways, 2006. Available from: https://mospace.umsystem.edu/xmlui/handle/10355/66819.

55. A. Yin, D. J. A. Moes, J. G. van Hasselt, J. J. Swen, H. J. Guchelaar, A review of mathematical models for tumor dynamics and treatment resistance evolution of solid tumors, *CPT Pharmacometrics Syst. Pharmacol.*, **8** (2019), 720–737. https://doi.org/10.1002/psp4.12450

56. C. A. Valentim Jr., N. A. Oliveira, J. A. Rabi, S. A. David, Can fractional calculus help improve tumor growth models, *J. Comput. Appl. Math.*, **379** (2020), 112964. https://doi.org/10.1016/j.cam.2020.112964

57. E. Ucar, N. Özdemir, E. Altun, Fractional order model of immune cells influenced by cancer cells, *Math. Model. Nat. Phenom.*, **14** (2019), 308. https://doi.org/10.1051/mmnp/2019002

58. S. Khajanchi, J. J. Nieto, Mathematical modeling of tumor-immune competitive system, considering the role of time delay, *Appl. Math. Comput.*, **340** (2019), 180–205. https://doi.org/10.1016/j.amc.2018.08.018

59. P. Unni, P. Seshaiyer, Mathematical modeling, analysis, and simulation of tumor dynamics with drug interventions, *Comput. Math. Methods Med.*, **2019** (2019), 4079298. https://doi.org/10.1155/2019/4079298

60. H. Y. Liu, H. L. Yang, L. G. Yang, Dynamics analysis in a tumor-immune system with chemotherapy, *Chin. Phys. B*, **30** (2021), 058201. https://doi.org/10.1088/1674-1056/abcf49

61. F. Subhan, M. A. Aziz, J. A. Shah, K. A. Kadir, I. M. Qureshi, Tumor treatment protocol by using genetic algorithm based Bernstein polynomials and sliding mode controller, *IEEE Access*, **9** (2021), 150192–150205. https://doi.org/10.1109/ACCESS.2021.3126491

62. K. C. Iarosz, F. S. Borges, A. M. Batista, M. S. Baptista, R. A. N. Siqueira, R. L. Viana, et al., Mathematical model of brain tumour with glia–neuron interactions and chemotherapy treatment, *J. Theor. Biol.*, **368** (2015), 113–121. https://doi.org/10.1016/j.jtbi.2015.01.006

63. J. Malinzi, R. Ouifki, A. Eladdadi, D. F. M. Torres, K. A. J. White, Enhancement of chemotherapy using oncolytic virotherapy: Mathematical and optimal control analysis, preprint, arXiv:1807.04329v1.
64. S. Khajanchi, M. Sardar, J. J. Nieto, Application of non-singular kernel in a tumor model with strong Allee effect, *Differ. Equations Dyn. Syst.*, **31** (2023), 687–692. https://doi.org/10.1007/s12591-022-00622-x
65. S. Sharma, G. P. Samanta, Analysis of the dynamics of a tumor–immune system with chemotherapy and immunotherapy and quadratic optimal control, *Differ. Equations Dyn. Syst.*, **24** (2016), 149–171. https://doi.org/10.1007/s12591-015-0250-1
66. J. M. J. da Costa, H. R. B. Orlande, W. B. da Silva, Model selection and parameter estimation in tumor growth models using approximate Bayesian computation-ABC, *Comput. Appl. Math.*, **37** (2017), 1–14. https://doi.org/10.1007/s40314-017-0479-0
67. D. S. Rodrigues, P. F. A. Mancera, Mathematical analysis and simulations involving chemotherapy and surgery on large human tumours under a suitable cell-kill functional response, *Math. Biosci. Eng.*, **10** (2013), 221–234. https://doi.org/10.3934/mbe.2013.10.221
68. L. G. Parajdi, R. Precup, M. A. Şerban, I. Ş. Haplea, Analysis of the effectiveness of the treatment of solid tumors in two cases of drug administration, *Math. Biosci. Eng.*, **18** (2021), 1845–1863. https://doi.org/10.3934/mbe.2021096
69. L. Berezansky, E. Braverman, L. Idels, Effect of treatment on the global dynamics of delayed pathological angiogenesis models, *Math. Biosci.*, **259** (2014), 34–48. https://doi.org/10.1016/j.mbs.2014.08.002
70. M. Alanazi, M. Bani-Yaghoub, B. B. C. Youan, Stable periodic solutions of a delayed reaction-diffusion model of Hes1-mRNA interactions, *Math. Biosci. Eng.*, **22** (2025), 2152–2175. https://doi.org/10.3934/mbe.2025079
71. O. Akinjole, K. Menta, A. Alsalhi, M. Bani-Yaghoub, B. B. C. Youan, Novel Meta-iodobenzylguanidine and Etoposide complex: Physicochemical characterization and mathematical modeling of anticancer activity, *AAPS PharmSciTech*, **24** (2023), 174. https://doi.org/10.1208/s12249-023-02599-4
72. M. Bani-Yaghoub, C. Ou, G. Yao, Delay-induced instabilities of stationary solutions in a single species nonlocal hyperbolic-parabolic population model, *Discrete Contin. Dyn. Syst.*, **13** (2020), 2509–2535. https://doi.org/10.3934/dcdss.2020195
73. M. Bani-Yaghoub, Analysis and applications of delay differential equations in biology and medicine, preprint, arXiv:1701.04173.
74. M. Bani-Yaghoub, Introduction to delay models and their wave solutions, preprint, arXiv:1701.04703.
75. M. Bani-Yaghoub, D. E. Amundsen, Dynamics of notch activity in a model of interacting signaling pathways, *Bull. Math. Biol.*, **72** (2010), 780–804. https://doi.org/10.1007/s11538-009-9469-8
76. M. A. Bani-Yaghoub, D. E. Amundsen, The role of Retinoic Acid and Notch in the symmetry breaking instabilities for axon formation, in *International Conference on Mathematical Biology, World Scientific and Engineering Academy and Society (WSEAS)*, 2006.

Appendix

A. Recent cancer models

Table A1 presents a comprehensive overview of recent cancer modeling studies, systematically categorized by model type. It highlights the primary objectives, methodologies, and key findings of each model, providing insights into their applications in tumor's growth dynamics, treatment strategies, and disease progression. This summary serves as a reference for comparing different modeling approaches and understanding their respective contributions to cancer research.

Table A1. Summary of recent cancer studies, their key findings, and model types.

Authors (year published)	Main result
Nonlinear ODE models	
Pinho et al. (2013) [15]	A five-equation model simulates tumor's growth dynamics, showing how anti-angiogenic agents enhance chemotherapy's effectiveness.
El Haout et al. (2021) [21]	The combination of immunotherapy and chemotherapy decreased tumor growth, with Heun's method providing the closest accuracy to the true value given by the Runge–Kutta output.
Sadeghi et al. (2021) [7]	The design is such that the volume of the cancerous tumor sharply reaches zero in finite time. Additionally, the chemotherapy injection rate was reduced by about 97%, and after a short period, the number of healthy cells returned to normal.
Hernandez-Rivera, et al. (2023) [3]	Modeling tumor growth can provide valuable insights into tumors' behavior, and it is crucial to incorporate sources of uncertainty to ensure that the models accurately capture tumor behavior.
Sharma et al. (2013) [13]	The optimal control is more effective in reducing the number of tumor cells to near zero.
Hanum et al. (2023) [8]	Reducing glioma endemicity among sensitive cases requires decreasing chemotherapy expenditure, increasing angiogenic dormancy, and adjusting chemotherapy infusion rates.
Sujitha et al. (2024) [11]	Numerical simulations of the model incorporating different treatment methods reveal the therapy's impact.
Sujitha, et al. (2023) [9]	Radiotherapy treatment lowers tumor development while enhancing glial cell proliferation, according to simulation results.
Kaviyan et al. (2023) [12]	The mathematical model shows the interplay between most cancer cells and immunotherapy.
Liu et al. (2021) [60]	The chaotic dynamics obtained in the model through equilibria analysis demonstrate the existence of chaos by calculating the Lyapunov exponents and the Lyapunov dimension of the system.

Continued on next page

Authors (year published)	Main result
Subhan et al. (2021) [61]	The hybrid approach in this research produces a potent minimization of cancer. The application of sliding mode controller (SMC). It is used as optimal control for normal and immune cells boosting in addition to escalated tumor minimization to ensure that the normal cell concentration stays well above the critical threshold, making a continuous treatment dose viable.
Ghasemabad et al. (2022) [14]	Simulation results and comparison studies show that adding anti-angiogenic treatment not only reduces chemotherapy's side effects and also that the proposed robust sliding mode controller provides faster and stronger treatment in the presence of patient-related parametric uncertainties.
Khalili et al. (2021) [20]	If an optimal controller could be designed to mix the advantages of both methods, the solution could widely be used to optimize drug injection rates and predict the system's dynamics in cancer treatment.
Samanta et al. (2017) [23]	Intervention practices involving periodically pulsed chemotherapy yield a better result in controlling tumor growth.
Shi et al. (2015) [40]	Anti-angiogenesis therapy cannot completely eliminate tumor cells; however, immunotherapy can eradicate tumor cells. Combined therapy achieves better therapeutic effects.
Iarosz et al. (2015) [62]	Chemotherapy can be applied while mitigating the side effects of drugs on neuron death. Infusion values were found for minimizing cancer's lifetime with less toxicity.
Malinzi et al. (2018) [63]	The analysis suggests that the optimal drug and virus combination corresponds to half their maximum tolerated doses.
Khajanchi1 et al. (2022) [64]	Analytical solutions were obtained in implicit form for a tumor cell population differential equation with a strong Allee effect.
Sharma et al. (2016) [65]	Immunotherapeutic drug control alone does not significantly alter tumor growth, but chemotherapeutic control alone does. Combining both yields rapidly reducing tumor cell populations.
Trobia et al. (2020) [37]	Continuous and pulsed chemotherapy can kill glioma cells with minimal neuron loss.
Yonucu et al. (2017) [39]	Large drug administration for targeted therapies should be combined with normalization for simultaneous access to both the tumor's rim and center.
Justino da Costa et al. (2017) [66]	The Monte Carlo approximate Bayesian computation (ABC) algorithm correctly selects the model and estimates the parameters used to generate the simulated measurements.
Rodrigues et al. (2013) [67]	Chemotherapy is less effective for tumors at plateau growth levels; a combination with surgical treatment yields better outcomes.

Continued on next page

Authors (year published)	Main result
Rodrigues et al. (2016) [24]	Metronomic schedules are more effective in eliminating tumor cells due to their impact on endothelial cells, with more frequent, low-dose regimens increasing patient's survival time.
Santurio et al. (2022) [19]	The model highlights CAR-T cell therapy's dynamics, providing insights into the consequences of "on-target" "off-tumor" effects, particularly in neuronal loss.
Urenda-Cázares et al. (2019) [22]	Combined therapy may reduce chemotherapy sessions, leading to better outcomes in glioma treatment.
Paradji et al. (2021) [68]	Mathematical analysis provides conditions for successful chemotherapy in terms of the mathematical relationships among parameters.
PDE & DDE models	
Berezansky, et al. (2016) [69]	Discusses the potential of continuous or impulse therapy to eradicate tumor cells and suppress angiogenesis.
Sujitha, et al. (2023) [10]	The analysis suggests that combination therapy could lead to tremendous success in treating gliomas.
Guiraldello, et al. (2016) [26]	The metronomic protocol is more effective than maximum tolerated dose (MTD) in prolonging patient's life. Uniform drug delivery combined with the metronomic protocol is the most efficient strategy to reduce tumor density.
Li (2016), et al. [25]	Time delay is harmless for the local and global dynamical properties of the model.

B. Components of the Jacobian matrix

The Jacobian matrix evaluated at the baseline equilibrium CPE is given by

$$J(\text{CPE}) = \begin{pmatrix} m_1 & m_2 & 0 & m_4 & m_5 \\ v_1 & v_2 & v_3 & v_4 & v_5 \\ 0 & g_2 & g_3 & 0 & g_5 \\ f_1 & f_2 & 0 & f_4 & 0 \\ 0 & 0 & z_3 & 0 & z_5 \end{pmatrix} \tag{B.1}$$

The components of the general Jacobian matrix of the proposed model are given by

$m_1 = \alpha_1 \left[r_1 c_1^{r_1 - 1} (1 - c_1)^{s_1} - c_1^{r_1} s_1 (1 - c_1)^{s_1 - 1} \right] - q_1 c_2 - \frac{p_1(c_3, \omega) y a_1}{(a_1 + c_1)^2}$

$m_2 = -q_1 c_1$

$m_4 = -\frac{p_1(c_3, \omega) c_1}{a_1 + c_1}$

$$m_5 = -\frac{c_1 * y * p_{12}}{a_1 + c_1}$$

$$v_1 = -q_2 c_1$$

$$v_2 = \alpha_2 (r_2 c_2^{r_2 - 1}) \left[1 - \frac{c_2}{1 + \gamma c_3}\right]^{s_2} + \alpha_2 c_2^{r_2} \left[s_2 \left(1 - \frac{c_2}{\gamma c_3}\right)\right]^{s_2 - 1} \left(\frac{-1}{1 + \gamma c_3}\right) - q_2 c_1 - \frac{p_2(c_3, \omega) y a_2}{(a_2 + c_2)^2}$$

$$v_3 = \alpha_2 c_2^{r_2} s_2 \left[1 - \frac{c_2}{1 + \gamma c_3}\right]^{s_2 - 1} \left(\frac{c_2 \gamma}{(1 + \gamma c_3)^2}\right)$$

$$v_4 = -\frac{p_2(c_3, \omega) c_2}{a_2 + c_2}$$

$$v_5 = \frac{p_{22} c_2 y}{a_2 + c_2}$$

$$g_2 = \beta$$

$$g_3 = -\alpha_3 (r_3 c_3^{r_3 - 1})(1 - c_3)^{s_3} + \alpha_3 c_3^{r_3} s_3 (1 - c_3)^{s_3 - 1} - \frac{p_3 \omega a_3}{(a_3 + c_3)^2}$$

$$g_5 = -\frac{p_3 c_3}{a_3 + c_3}$$

$$f_1 = \frac{y d_1 a_1}{(a_1 + c_1)^2}$$

$$f_2 = \frac{y d_2 a_2}{(a_2 + c_2)^2}$$

$$f_4 = -\left(\varepsilon + \frac{d_1 c_1}{a_1 + c_1} + \frac{d_2 c_2}{a_2 + c_2}\right)$$

$$z_3 = \frac{a_3 \omega}{(a_3 + c_3)^2}$$

$$z_5 = -\left(\eta + \frac{a_3 c_3}{a_3 + c_3}\right)$$

C. Further details on the numerical bifurcation analysis

Figure A1 presents the results of numerical bifurcation analysis results under varying values of the parameters r_1 and r_2, which influence cell proliferation and cancer cell death, respectively. The figures illustrate the spatial distributions of (a) healthy cells, (b) cancer cells, (c) endothelial cells, and (d) the chemotherapy agent. The model demonstrates greater sensitivity to r_1 than to r_2; specifically, healthy cells are eliminated when $r_1 > 2$, while cancer cell death becomes more pronounced when $r_1 > 4.6$ and r_2 is low. The immune response increases as cancer cells' density rises, yet chemotherapy concentrations remain relatively unchanged within the tested parameter range.

Figure A2 explores the influence of the parameters s_1 and s_2 on tumor dynamics. The figures show the distributions of (a) healthy cells, (b) cancer cells, (c) endothelial cells, and (d) the chemotherapy agent. Increasing s_1 leads to a reduction in healthy cells, while the model exhibits limited sensitivity to s_2. Compared with to the r_1–r_2 pair, the s_1–s_2 combination is less effective in suppressing cancer cells.

An increase in immune activity with higher cancer densities is again observed. Similar to Figure A1, chemotherapy concentrations are minimally affected by parameter variations within the range tested.

Figure A3 depicts tumor progression in the absence of all treatments—chemotherapy, immunotherapy, and anti–angiogenic therapy—under Stage 4 cancer conditions. The tumor exhibits unchecked growth, highlighting the aggressive nature of advanced-stage cancer and the critical importance of therapeutic intervention.

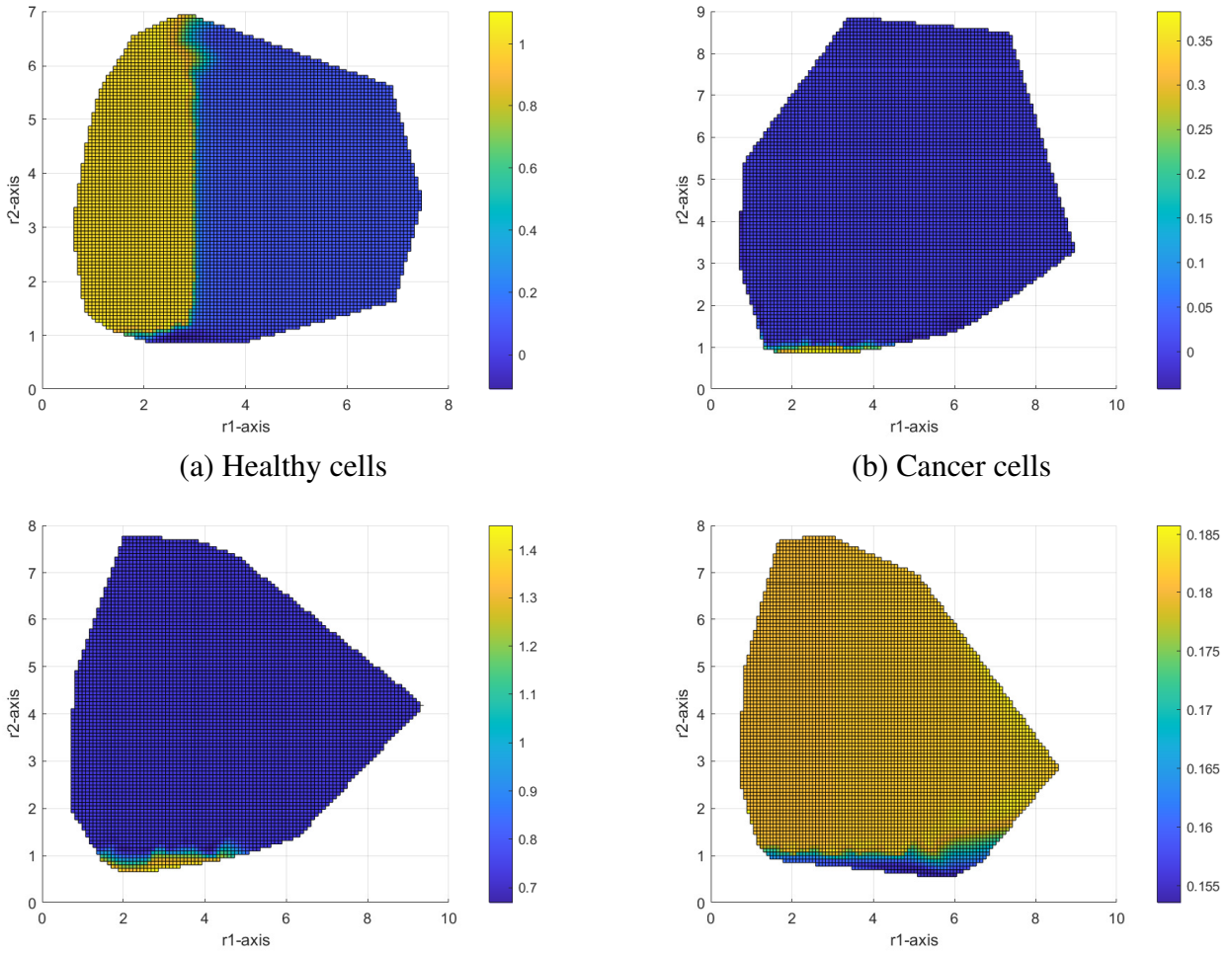

(a) Healthy cells

(b) Cancer cells

(c) Endothelial cells

(d) Chemotherapy agent

Figure A1. The model shows greater sensitivity to the values of r_1 than r_2. Specifically, r_1 values must remain below 2 to prevent the death of healthy cells; r_2, which promotes cancer cells' death, becomes more impactful when r_1 exceeds 4.6. Furthermore, higher cancer cell densities lead to an increase in the immune response, which is expected. However, on a scale of 0.155–0.185 on the color bar, the concentration of the chemotherapy agent does not significantly change when r_1 and r_2 increase.

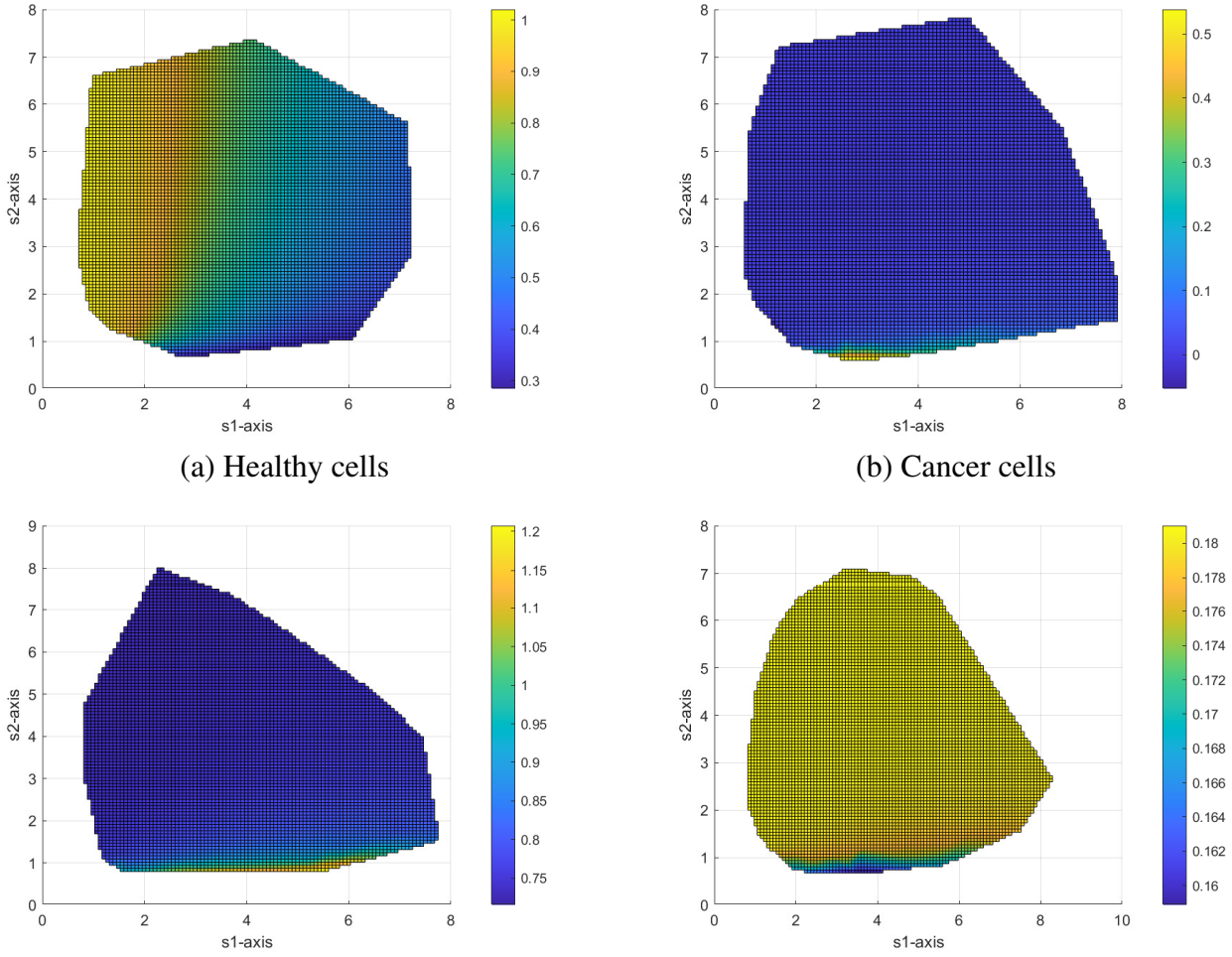

(a) Healthy cells

(b) Cancer cells

(c) Endothelial cells

(d) Chemotherapy agent

Figure A2. As s_1 increases, healthy cells decrease, and the model is less sensitive to s_2. The r_1 and r_2 combination is far more effective at eliminating cancer cells than the s_1 and s_2 combination. Specifically, cancer cells die when $r_1 > 4.6$ and $r_2 < 1$. There is an expected increase in immune response with higher cancer cell densities. According to the color bar scale of 0.16–0.18, there is no significant impact on the concentration of the chemotherapy agent when s_1 and s_2 increase.

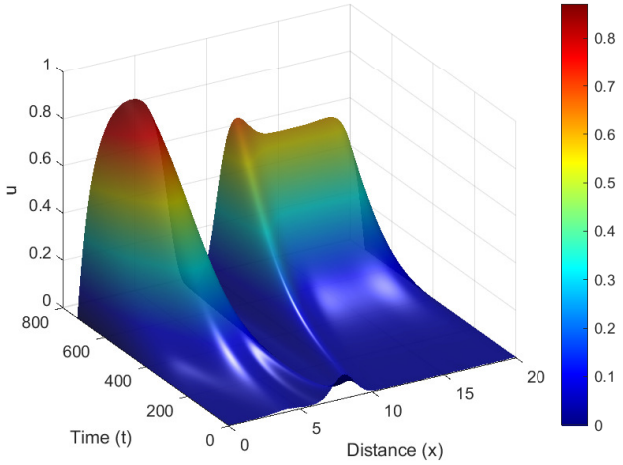

Figure A3. This figure shows the progression of the tumor with no treatment (no chemotherapy, no immunotherapy, no anti–angiogenic therapy), where the tumor increases significantly, indicating the severity of Stage 4 cancer without any intervention.

D. Simulations of different stages of cancer

Table A2. Summary of key findings from spatio–temporal model simulations associated with different stages of cancer.

Treatment	Outcome
Stage 1 (tumor < 2 cm)	
With chemotherapy	The area under the curve shows a decrease throughout the 50 days. Tumor size significantly reduces after 50 days. After 32 days, the tumor size falls below 1% of its original size.
Without chemotherapy	The area of the tumor grows by 38%. The area of the tumor increases as time increases.
Stage 2 (tumor 3–5 cm)	
With chemotherapy	Slower decline in the tumor size compared with Stage 1. After 60 days, there was a successful reduction in the tumor size. After 35 days, the tumor size falls below 1% of its original size.
Without chemotherapy	The tumor grows by 30%, emphasizing the need for chemotherapy in this stage.
Stage 3 (tumor > 5 cm)	
With chemotherapy and anti–angiogenic therapy	After 61 days, the tumor size falls below 1% of its original size and there is full recovery after 110 days.
With chemotherapy and no anti–angiogenic therapy	There is a reduction for the first 160 days, but after that, the tumor size stays the same as its size.

Continued on next page

Stage	Outcomes
Only anti–angiogenic therapy	The tumor grows by 209% with only anti–angiogenic therapy, indicating the crucial role of chemotherapy.
no therapy	Without intervention, the tumor grows by 421%, which is expected at an advanced stage.
Stage 4 (varying sizes)	
With chemotherapy, immunotherapy, and anti–angiogenic therapy	After 132 days, the tumor size falls below 1% of its original size. There is full recovery after about 200 days.
With immunotherapy and anti–angiogenic therapy	Tumor size decreases by 76% by the 730 days.
With chemotherapy and immunotherapy	Tumor size decreases by 84% after 724 days. The effect of this combination on the tumor size is more effective than the previous combination.
With chemotherapy and anti–angiogenic therapy	Tumor size decreases by 87% after 718 days, demonstrating that chemotherapy and anti–angiogenic therapy are more effective than the other combinations.
No therapy	Without any intervention, the tumor grows excessively, which is expected, as this is the most severe stage of cancer without treatment.

E. Stability of analysis with the presence of diffusion for the five CPE types of equilibria

Corollary 6 (Stability of CFE Type 1 with diffusion)**.** *Let $p_1 > 0$ and $p_3 > 0$. Assume the following:*

(H_1) $a_3 = 0$ and $d_1 = 0$,

(H_2) $m_1 + v_2 < 0$, and

(H_3) $m_1 v_2 - m_2 v_1 > 0$

In this case, in the presence of diffusion, the cancer-free equilibrium (Type 1) $CPE^{[1]} = (c_1^{[1]}, 0, c_3^{[1]}, y^{[1]}, \omega^{[1]})$ remains locally asymptotically stable for all $k \in \mathbb{R}$.

Proof. Under Hypothesis H_1, we have $f_1 = 0$ and $z_3 = 0$, which simplifies the characteristic polynomial of the Jacobian to

$$(g_3 - \lambda)(z_5 - \lambda)(f_4 - \lambda)\left((m_1 - \lambda)(v_2 - \lambda) - m_2 v_1\right).$$

With diffusion, the Jacobian becomes $J_k = J(CPEtype1) - k^2 D$, where D is the diagonal matrix of the diffusion coefficients. This modifies the characteristic polynomial where g_3 becomes $g_3 - D_3 k^2, z_5 = z_5 - D_5 k^2, f_4 = f_4 - D_4 k^2$, and $v_2 = v_2 - D_2 k^2$.

Thus the modified characteristic polynomial becomes

$$(g_3 - D_3 k^2 - \lambda)(z_5 - D_5 k^2 - \lambda)(f_4 - D_4 k^2 - \lambda)\left((m_1 - \lambda)(v_2 - D_2 k^2 - \lambda) - m_2 v_1\right).$$

The first three eigenvalues are

$$\lambda_1 = g_3 - D_3 k^2, \quad \lambda_2 = z_5 - D_5 k^2, \quad \lambda_3 = f_4 - D_4 k^2.$$

Since $g_3, z_5, f_4 < 0$ by assumption, and $D_i \geq 0$, these eigenvalues remain negative for all $k \geq 0$.

The last two eigenvalues come from the quadratic

$$\lambda^2 - (m_1 + v_2 - D_2k^2)\lambda + (m_1(v_2 - D_2k^2) - m_2v_1).$$

The new coefficients still satisfy the Routh–Hurwitz conditions:

The trace ($m_1+v_2-D_2k^2 < 0$) for all k, because $m_1+v_2 < 0$ by (H_2), and subtracting $D_2k^2 \geq 0$ preserves negativity.

The determinant becomes

$$m_1(v_2 - D_2k^2) - m_2v_1.$$

Since $D_2k^2 \geq 0$ and $m_1(v_2 - D_2k^2) < m_1v_2$, the term is slightly reduced. But the original expression $m_1v_2 - m_2v_1 > 0$ by (H_3), so for a sufficiently small D_2, this remains positive. Hence, both eigenvalues retain negative real parts.

Therefore, all five eigenvalues have negative real parts and the equilibrium $CPE^{[1]}$ remains locally asymptotically stable in the presence of diffusion for all $k \in \mathbb{R}$.

Corollary 7 (Stability of CFE Type 2 with diffusion)**.** *Assume the non-diffusive cancer-free equilibrium Type 2 ($CPE^{[2]}$) is locally asymptotically stable, that is, the coefficients q_4, q_3, q_2, q_1, q_0 satisfy*

(i) $q_4 > 0, \quad q_3 > 0, \quad q_2 > 0, \quad q_1 > 0, \quad q_0 > 0$;

(ii) $q_4q_3q_2 > q_2^2 + q_4^2q_1$;

(iii) $(q_4q_1 - q_0)(q_4q_3q_2 - q_2^2 - q_4^2q_1) > q_0(q_4q_3 - q_2)^2 + q_4q_0^2$

where

$$\begin{aligned}
q_4 &= f_4 + g_3 + m_1 + v_2 + z_5,\\
q_3 &= -(f_4g_3 + f_4m_1 + f_4v_2 + f_4z_5 + g_3m_1 + g_3v_2 + g_3z_5 - g_5z_3 + m_1v_2 + m_1z_5 - m_2v_1 + v_2z_5),\\
q_2 &= f_4g_3m_1 + f_4g_3v_2 + f_4g_3z_5 - f_4g_5z_3 + f_4m_1v_2 + f_4m_1z_5 - f_4m_2v_1 + f_4v_2z_5\\
&\quad + g_3m_1v_2 + g_3m_1z_5 - g_3m_2v_1 + g_3v_2z_5 - g_5m_1z_3 - g_5v_2z_3 + m_1v_2z_5 - m_2v_1z_5,\\
q_1 &= -(f_4g_3m_1v_2 + f_4g_3m_1z_5 - f_4g_3m_2v_1 + f_4g_3v_2z_5 - f_4g_5m_1z_3 - f_4g_5v_2z_3\\
&\quad + f_4m_1v_2z_5 - f_4m_2v_1z_5 + g_2m_5v_1z_3 - g_3m_1v_2z_5 + g_3m_2v_1z_5 + g_5m_1v_2z_3 - g_5m_2v_1z_3),\\
q_0 &= -f_4g_2m_5v_1z_3 + f_4g_3m_1v_2z_5 - f_4g_3m_2v_1z_5 - f_4g_5m_1v_2z_3 + f_4g_5m_2v_1z_3.
\end{aligned}$$

Then for all $k \geq 0$, the diffusion-modified Jacobian $J_k = J - k^2D$ has eigenvalues with negative real parts. That is, CFE Type 2 remains locally asymptotically stable in the full reaction–diffusion system, and no diffusion-driven instability occurs.

Proof. Let the Jacobian matrix evaluated at $CPE^{[2]} = (1, 0, c_3^{[2]}, 0, \omega^{[2]})$ be denoted by

$$J = \begin{pmatrix} m_1 & m_2 & 0 & m_4 & 0\\ v_1 & v_2 & 0 & 0 & 0\\ 0 & g_2 & g_3 & 0 & g_5\\ 0 & 0 & 0 & f_4 & 0\\ 0 & 0 & z_3 & 0 & z_5 \end{pmatrix}$$

Assume that each diffusing component has the diffusion coefficient $D_i \geq 0$.

We define the diffusion-adjusted characteristic polynomial at each mode $k \geq 0$ as:

$$\lambda^5 + q_4^{[k]}\lambda^4 + q_3^{[k]}\lambda^3 + q_2^{[k]}\lambda^2 + q_1^{[k]}\lambda + q_0^{[k]} = 0$$

Each coefficient $q_j^{[k]}$ is a continuous and monotonically increasing function of q_j with additional positive terms from the diffusion contributions $k^2 D_j$. That is

$$q_j^{[k]} = q_j + D_j k^2, \quad \text{with} D_j k^2 \geq 0$$

Because the non–diffusive system satisfies the Routh–Hurwitz conditions (i)–(iii), and the added diffusion terms only strengthen the inequalities, the Routh–Hurwitz conditions remain satisfied for all $k \geq 0$. Thus for each $q_j^{[k]} > q_j > 0$, Condition (i) remains true and Conditions (ii) and (iii) involve polynomial inequalities that are strengthened by the positive additive diffusion terms.

Thus, for all $k \in \mathbb{R}$, the eigenvalues of $J - k^2 D$ have negative real parts. Therefore, CPE Type 2 remains locally asymptotically stable in the presence of diffusion.

Corollary 8 (Stability of CFE Type 3 with diffusion)**.** *The cancer-free equilibrium (Type 3) exists if p_1 is sufficiently small. In the presence of diffusion, the equilibrium*

$$CPE^{[3]} = (c_1^{[3]}, 0, c_3^{[3]}, y^{[3]}, \omega^{[3]})$$

is locally asymptotically stable for all $k \geq 0$, provided the following Routh–Hurwitz conditions hold:

(i) $t_1^{[k]} > 0$

(ii) $t_3^{[k]} > 0$

(iii) $t_1^{[k]} t_2^{[k]} > t_3^{[k]}$

where the diffusion-modified coefficients are

$$\begin{aligned}
t_1^{[k]} &= -(m_1 + v_2 + f_4 + D_1 k^2 + D_2 k^2 + D_4 k^2), \\
t_2^{[k]} &= -(f_1 m_4 - m_1 v_2 - f_4 m_1 - f_4 v_2 + m_2 v_1) - (D_1 D_2 + D_1 D_4 + D_2 D_4) k^4, \\
t_3^{[k]} &= f_1 m_4 v_2 - f_4 m_1 v_2 + f_4 m_2 v_1 \\
&\quad + k^2 (D_1 m_4 v_2 + f_1 D_4 v_2 + f_1 m_4 D_2 - D_4 m_1 v_2 - f_4 D_1 v_2 - f_4 m_1 D_2 \\
&\quad + D_4 m_2 v_1 + f_4 D_1 v_1 + f_4 m_2 D_2) + D_1 D_2 D_4 k^6.
\end{aligned}$$

Proof. With diffusion, the Jacobian becomes $J_k = J(CPE^{[3]}) - k^2 D$, where

$$D = \text{diag}(0, D_2, D_3, D_4, D_5),$$

$CPE^{[3]}$ becomes

$$J_k = \begin{pmatrix} m_1 & m_2 & 0 & m_4 & m_5 \\ v_1 & v_2 - D_2 k^2 & 0 & 0 & 0 \\ 0 & g_2 & g_3 - D_3 k^2 & 0 & g_5 \\ f_1 & 0 & 0 & f_4 - D_4 k^2 & 0 \\ 0 & 0 & 0 & 0 & z_5 - D_5 k^2 \end{pmatrix}$$

The characteristic polynomial factorizes as

$$(g_3 - D_3k^2 - \lambda)(z_5 - D_5k^2 - \lambda) \cdot P_k(\lambda),$$

The first two eigenvalues are

$$\lambda_1 = g_3 - D_3k^2, \qquad \lambda_2 = z_5 - D_5k^2.$$

Under the assumptions that $g_3 < 0, z_5 < 0$, and $D_3, D_5 > 0$, these eigenvalues remain negative for all $k \geq 0$. The remaining cubic is

$$P_k(\lambda) = -\lambda^3 + t_1^{[k]}\lambda^2 + t_2^{[k]}\lambda + t_3^{[k]}.$$

Multiplying by -1, the cubic takes standard Routh–Hurwitz form

$$\lambda^3 + t_1^{[k]}\lambda^2 + t_2^{[k]}\lambda + t_3^{[k]}.$$

Since $t_i, i = 1, 2, 3$, the non–diffusive coefficients is assumed to satisfy

$$t_1 > 0, \quad t_3 > 0, \quad t_1t_2 > t_3,$$

With $t_1^{[k]} > t_1 > 0$ $t_3^{[k]} > t_3 > 0$. Since $t_2^{[k]} > t_2$, the inequality $t_1^{[k]}t_2^{[k]} > t_3^{[k]}$ continues to hold.

Thus, the Routh–Hurwitz conditions are preserved under diffusion.

Therefore, the eigenvalues have negative real parts for all $k \geq 0$, and the CFE Type 3 is locally asymptotically stable in the presence of diffusion.

Corollary 9 (Stability of CFE Type 4 with diffusion)**.** *The cancer-free equilibrium (Type 4)*

$$CPE^{[4]} = (c_1^{[4]}, 0, c_3^{[4]}, 0, 0),$$

is locally asymptotically stable in the presence of diffusion for all $k \geq 0$, provided that the following conditions are satisfied:

(i) $(v_2 - D_2k^2) < 0$,

(ii) $m_2v_1 < 0$,

(iii) $f_4 < 0, \quad z_5 < 0, \quad D_4 > 0, \quad D_5 > 0$.

Proof. At the CFE Type 4, the values $c_2^{[4]} = y^{[4]} = \omega^{[4]} = 0$ imply that both $c_1^{[4]}$ and $c_3^{[4]}$ approach their maximal values which is (assumed to be normalized to 1). Evaluating the Jacobian matrix with diffusion gives

$$J_k(CPE^{[4]}) = \begin{pmatrix} 0 & m_2 & 0 & m_4 & 0 \\ v_1 & v_2 - D_2k^2 & 0 & 0 & 0 \\ 0 & g_2 & -D_3k^2 & 0 & g_5 \\ 0 & 0 & 0 & f_4 - D_4k^2 & 0 \\ 0 & 0 & 0 & 0 & z_5 - D_5k^2 \end{pmatrix}$$

The characteristic polynomial factors into

$$(f_4 - D_4k^2 - \lambda)(z_5 - D_5k^2 - \lambda) \cdot P_k(\lambda),$$

where

$$P_k(\lambda) = \lambda^3 - (v_2 - D_2k^2)\lambda^2 - m_2v_1\lambda.$$

$$\lambda_1 = f_4 - D_4k^2, \qquad \lambda_2 = z_5 - D_5k^2.$$

Given that $f_4 < 0$, $z_5 < 0$, and $D_4, D_5 > 0$, these eigenvalues are negative for all $k \geq 0$.

$$P_k(\lambda) = \lambda^3 - (v_2 - D_2k^2)\lambda^2 - m_2v_1\lambda.$$

This simplifies to

$$\lambda^2 - (v_2 - D_2k^2)\lambda - m_2v_1.$$

By the Routh–Hurwitz criterion, it follows that all eigenvalues of the full Jacobian matrix J_k have negative real parts for all $k \geq 0$.

Hence, the cancer-free equilibrium Type 4 remains locally asymptotically stable in the presence of diffusion.

Corollary 10 (Stability of CFE Type 5 with diffusion)**.** *Assume the non–diffusive cancer-free equilibrium (CFE Type 5) is locally asymptotically stable, that is, the characteristic polynomial*

$$\lambda^5 + b_4\lambda^4 + b_3\lambda^3 + b_2\lambda^2 + b_1\lambda + b_0 = 0$$

satisfies the Routh–Hurwitz conditions

(i) $b_4 > 0, \quad b_3 > 0, \quad b_2 > 0, \quad b_1 > 0, \quad b_0 > 0,$

(ii) $b_4b_3b_2 > b_2^2 + b_4^2b_1,$

(iii) $(b_4b_1 - b_0)(b_4b_3b_2 - b_2^2 - b_4^2b_1) > b_0(b_4b_3 - b_2)^2 + b_4b_0^2.$

Then for all $k \geq 0$, $J_k = J(CPE^{[5]}) - k^2D$ yields a characteristic polynomial of the form

$$\lambda^5 + b_4^{[k]}\lambda^4 + b_3^{[k]}\lambda^3 + b_2^{[k]}\lambda^2 + b_1^{[k]}\lambda + b_0^{[k]} = 0,$$

where each $b_i^{[k]}$ is a continuous, increasing function of k^2, due to the non-negative diffusion terms added to the diagonal entries.

Then all eigenvalues of the Jacobian J_k have negative real parts for all $k \geq 0$.

Proof. Let the characteristic polynomial be

$$\lambda^5 + b_4^{[k]}\lambda^4 + b_3^{[k]}\lambda^3 + b_2^{[k]}\lambda^2 + b_1^{[k]}\lambda + b_0^{[k]} = 0,$$

where each $b_i^{[k]}$ is a continuous function of k^2 with

$$b_i^{[k]} = b_i + D_ik^2 \quad \text{and} \quad D_ik^2 \geq 0 \quad \text{for all} \quad k \geq 0 \quad \text{and} \quad i = 0, 1, 2, 3, 4.$$

By assumption, the non–diffusive coefficients b_i satisfy the strict Routh–Hurwitz conditions:

(i) $b_4, b_3, b_2, b_1, b_0 > 0,$

(ii) $b_4b_3b_2 > b_2^2 + b_4^2b_1,$

(iii) $(b_4b_1 - b_0)(b_4b_3b_2 - b_2^2 - b_4^2b_1) > b_0(b_4b_3 - b_2)^2 + b_4b_0^2.$

Since $D_i k^2$ are non-negative and smooth in k, all inequalities remain satisfied for $b_i^{[k]}$. Therefore, the Routh-Hurwitz conditions hold for all $k \geq 0$, and all eigenvalues have negative real parts.

Hence, the cancer-free equilibrium Type 5 remains locally asymptotically stable under diffusion.

F. Simulation of the stability of the ODE and full PDE systems

To complement the local stability analysis of the spatially homogeneous system, we performed numerical simulations to investigate the stability behavior both in the absence and presence of diffusion, specifically the baseline equilibrium. These simulations validate the analytical results by illustrating the system dynamics for the ODE model and the full reaction–diffusion PDE system.

Figure A4 shows that the eigenvalues of the ODE Jacobian ($k = 0$) indicate that the homogeneous equilibrium is locally asymptotically stable, i.e., all eigenvalues have negative real parts.

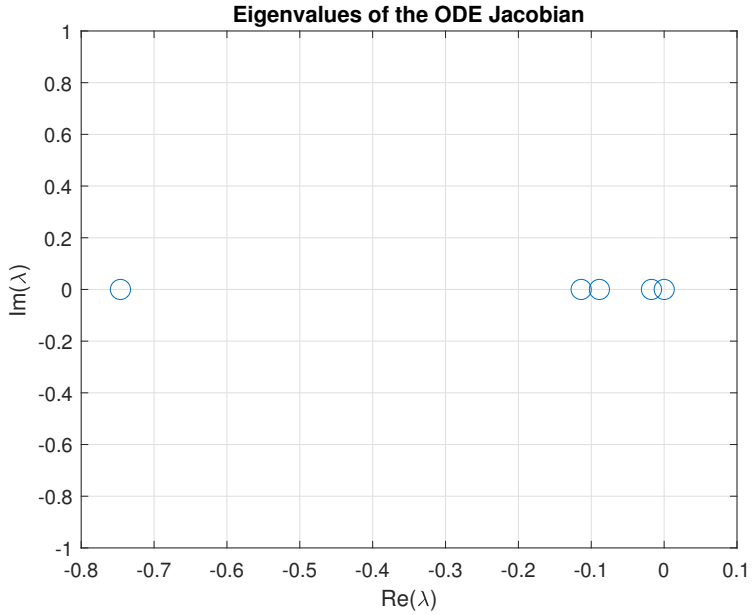

Figure A4. Eigenvalues of the Jacobian matrix for the ODE system evaluated at the homogeneous equilibrium. All real parts are negative, confirming local stability.

In Figure A5, we plot the real part of the leading eigenvalue as a function of the spatial wavenumber k (the dispersion relation). The result shows that $\mathrm{Re}(\lambda_{\max}(k)) < 0$ for all $k \in [0, 2]$, thus ruling out Turing-type instabilities. The system remains linearly stable under spatial perturbations, as shown analytically.

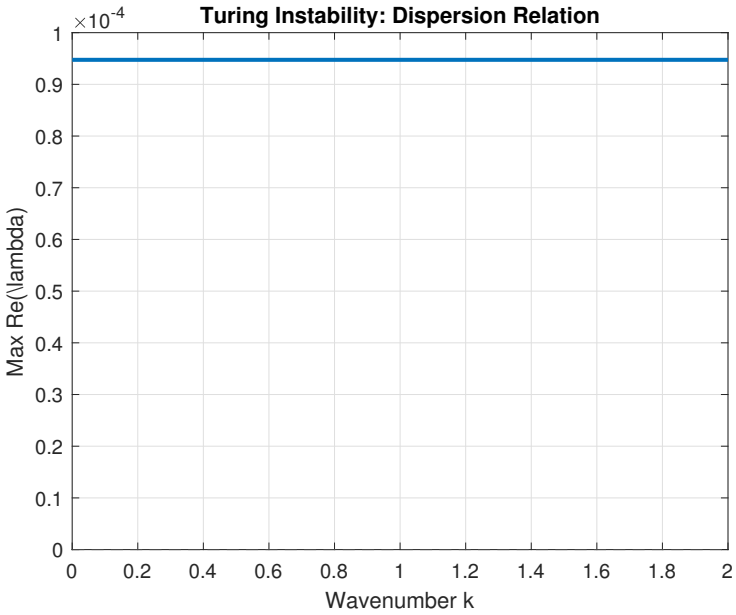

Figure A5. Dispersion relation showing $\max \mathrm{Re}(\lambda(k))$ for $k \in [0, 2]$. No wavenumber leads to a positive growth rate, indicating absence of diffusion-driven instability.

These numerical results confirm that the equilibrium is stable both for the ODE and PDE systems. This strengthens our analytical conclusions and rules out Turing-type dynamics in the biologically relevant parameter regimes considered.